REV00
2/14/05

Estimating Liquid Fluxes in Thermally Perturbed Fractured Rock Using Measured Temperature Profiles

Jens T. Birkholzer
Ernest Orlando Lawrence Berkeley National Laboratory (LBNL)
1 Cyclotron Road
Berkeley CA 94720
phone 5104867134, fax 5104865686, jtbirkholzer@lbl.gov

Abstract: A new temperature-profile method was recently developed for analyzing perturbed flow conditions in superheated porous media. The method uses high-resolution temperature data to estimate the magnitude of the heat-driven liquid and gas fluxes that form as a result of boiling, condensation, and recirculation of pore water. In this paper, we evaluate the applicability of this new method to the more complex flow behavior in fractured formations with porous rock matrix. In such formations, with their intrinsic heterogeneity, the porous but low-permeable matrix provides most of the mass and heat storage capacity, and dominates conductive heat transfer. Fractures, on the other hand, offer highly effective conduits for gas and liquid flow, thereby generating significant convective heat transfer. After establishing the accuracy of the temperature-profile method for fractured porous formations, we apply the method in analyzing the perturbed flow conditions in a large-scale underground heater test conducted in unsaturated fractured porous tuff. The flux estimates for this test indicate a signifcant reflux of water near the heat source, on the order of a few hundred millimeter per year—much larger than the ambient percolation flux of only a few millimeter per year.

Key Words: heat, flow, fractured rock, temperature profile, thermal perturbation

1. Introduction

Evaluating the magnitude of flux perturbation in superheated subsurface systems can be a challenging task, in part because the direct *in situ* measurement of such quantities is virtually impossible. Flux perturbations are particularly strong in geologic heat pipes, where vapor is transported away from the heat source while condensate water flows back towards the heat source, thereby creating a continuous recirculation of vapor and water at significant rates (e.g., Udell, 1985; Doughty and Pruess, 1990, 1992). Examples of geologic heat pipes can be found in geothermal systems, near emplacement tunnels for the disposal of heat-producing nuclear wastes, in the vicinity of buried pipelines and electrical cables, in post-accident sites with boiling of fluids from nuclear reactor debris, and in oil fields as a result of thermally enhanced recovery (Udell, 1985).

Of specific concern in this paper is the expected flux perturbation in the vicinity of the geologic repository for nuclear waste at Yucca Mountain, Nevada (Pruess et al., 1990a, 1990b), where the decaying radioactive material produces significant amounts of heat. Determining the two-phase flow conditions in the fractured porous rock at Yucca Mountain is relevant to the performance of this repository, because these conditions affect the temperature and relative humidity close to the waste packages—important parameters for their corrosion. Large-scale heater tests have been conducted in underground research tunnels at Yucca Mountain to assess the future repository's response to the decay heat and to determine the impact of thermal perturbation on liquid and gas flow. These tests show clear evidence of heat-pipe behavior in the fractured porous rock (e.g., Birkholzer and Tsang, 2000; Bechtel SAIC Company, 2004a).

Temperature-profile methods have been employed since the early 1960s to better understand the magnitude of subsurface flows. For example, Bredehoeft and Papadopolous (1965), and more recently Constantz et al. (2003), estimated the percolation fluxes in vadose environments, using measured deviations from the conduction-only geothermal gradient to evaluate the rate of convective heat transport with the percolating water. Temperature profiles have also been used for examining stream/ground water interactions (e.g., Silliman et al., 1995; Constantz and Thomas, 1996) and for estimating the vertical hydraulic conductivity in stream/aquifer systems (Su et al., 2004), through analysis of subsurface temperature data as influenced by the natural variation of stream temperature patterns.

Whereas the above-mentioned studies addressed ambient flow systems with relatively low temperature ranges, a new temperature-profile method was recently developed to estimate the heat-driven fluxes in geologic heat pipes forming near superheated subsurface systems (Birkholzer, 2004). The method is based on the observation that the energy required for the vaporization of water can be estimated from the difference in the temperature gradients within and outside of the heat pipe. Once the boiling energy has been determined, the amount of water reflux in the heat pipe can be easily calculated from thermodynamic principles. Birkholzer (2004) demonstrated the potential of the new method for various example cases with geologic heat pipes situated in a porous media setting.

The objective of this study is to investigate whether the temperature-profile method of Birkholzer (2004) can also be applied to the more complex thermal-hydrological conditions in fractured formations with a porous, low-permeability rock matrix. Such formations are intrinsically heterogeneous, creating a significantly more complex flow and transport behavior that is affected by local temperature, pressure, and saturation differences between the matrix blocks and the surrounding fractures. We will demonstrate that the temperature-profile method works well in these specific conditions, and that the estimated fluxes derived from temperature gradients represent the combined reflux in the fractures and matrix blocks. In the following sections, we briefly review the general basis for the proposed temperature-profile method of Birkholzer (2004), discuss the specific heat-pipe conditions in fractured porous rock, test the method in comparison with a numerical solution of thermally driven flow processes in a hypothetical fractured formation, and finally present a sample application using the measured temperature profiles from a large-scale underground heater test conducted in the fractured tuff at Yucca Mountain, Nevada.

2. Brief Review of the Temperature-Profile Method

The temperature-profile method developed by Birkholzer (2004) takes advantage of the fact that the vapor-liquid flow processes within a heat pipe transmit a significant amount of energy. This creates a nearly isothermal zone maintained at about the boiling temperature, with temperature gradients much smaller than those in the surrounding conduction-dominated regions. The differences between the temperature gradients measured inside and outside of a heat pipe were shown to be proportional to the amount of energy available to vaporize water, which in turn was used to estimate the amount of thermally driven water flux in the heat pipe region (Birkholzer, 2004). Below, we briefly discuss the basic flow and transport behavior in geologic heat pipes, followed by a short review of the governing equations developed for the temperature-profile method.

2.1 Basic Characteristics of Geologic Heat Pipes

Geologic heat pipes create a distinct signature in temperature profiles, which can be measured and detected in the field with relative ease. This distinct signature is schematically illustrated in Figure 1, where temperature is plotted as a function of distance from a heat source emplaced in a partially saturated subsurface environment. The figure shows a situation with temperature above the boiling point of water near the heat source, corresponding to a zone of zero saturation where most of the pore water has boiled off. Heat transfer in this zone is conduction-dominated; thus, it is referred to hereafter as the inner conduction zone. The heat pipe region is clearly identifiable by the almost-zero temperature gradient at about the boiling temperature of water. The temperature plateau is generated by significant convective transport of heat, a result of

the counterflow of vapor and water. As water boils off at the hot end of the heat pipe, gas pressure builds up and causes vapor transport away from the heater. The vapor condenses in sub-boiling temperature regions and deposits a large amount of latent heat at the cool end of the heat pipe. Condensation gives rise to an increase in saturation at this location, creating a capillary pressure gradient that drives the reflux of liquid water back to the heat source. Gravity effects may amplify the magnitude of reflux. As the water is driven back to the hot end of the heat pipe, it vaporizes again and repeats the cycle. This cyclic flow in heat pipes can generate vapor and water fluxes orders of magnitude higher than at ambient conditions. The larger the vapor-water counterflow in a heat pipe, the more heat is transferred by convection, and the stronger the effect on the temperature profile.

In the literature, heat pipes are often treated as steady-state systems, meaning that the location and intensity of the heat pipe does not vary with time (stationary heat pipes). In this case, the energy conducted from the heat source to the heat pipe region would be fully consumed for the vaporization of refluxing water. However, whereas the steady-state assumption is justified for most engineered heat pipe devices, the heat pipes observed in geologic systems are often transient systems; i.e., they slowly move away from the heat source and transport the regions of vaporization and condensation further outward. In this case, the energy provided by the heat source is not only needed to vaporize refluxing water, but also to change the temperature in the solid phase and to boil the resident pore water in the system as the heat pipe migrates.

2.2 Calculating Water Reflux with the Temperature-Profile Method

The governing equations for the temperature-profile method are based on simple one-dimensional mass- and energy-balance formulations for a finite volume, as depicted in Figure 1. The finite volume incorporates small portions of rock at the hot end of the heat pipe, with one side situated in the inner conduction zone (featuring a large temperature gradient ∇T_1) and the other side situated within the heat-pipe region (featuring a small temperature gradient ∇T_2). As pointed out in Birkholzer (2004), the finite volume is always vapor dominated, meaning that the component air can be neglected in the formulations. (Consequently, the terms "vapor" and "gas" are used interchangeably in this paper.) Balancing the mass and heat flow components for the finite volume results in a set of equations that link the magnitude of the water reflux q_L to the difference in the temperature gradients measured at both sides of the finite volume. Birkholzer (2004) provided solutions for q_L for stationary as well as transient heat pipes assuming simplified geometrical conditions with one-dimensional heat and mass flow, one for radial-symmetric geometry, one for linear geometry.

For stationary heat pipes in a radial-symmetric system, the water reflux q_L^S towards the boiling region in a heat pipe was approximately given as (Birkholzer, 2004)

$$q_L^S \approx \frac{\left(r_1 \lambda_1 \nabla T_1 - r_2 \lambda_2 \nabla T_2\right)}{r_2 \rho_L \left(h_G - h_L\right)}. \tag{1}$$

Equation (1), referred to hereafter as the quasi-steady solution, contains either site-specific quantities that can be easily determined from laboratory and field measurements

(e.g., distance of finite volume from the heat source, as expressed by the radii r_1 and r_2 measured at both sides of the finite volume; temperature gradients ∇T_1 and ∇T_2; thermal conductivities λ_1 and λ_2) or known thermodynamic properties of water and vapor (water density ρ_L; specific enthalpies of gas h_G and water h_L). The thermodynamic properties ρ_L, h_G, and h_L can be assumed constant within the finite volume, because there are no drastic changes in temperature and pressure. Note the convention of positive fluxes moving outward, in a positive *r*-direction. Thus, liquid fluxes directed back towards the heat source would come out as negative values according to this convention. At steady-state conditions, in which the storage terms in the mass and energy balance equations can be neglected, the gas flux has identical magnitude, but opposite direction to the liquid flux ($q_G^S = -q_L^S$).

Birkholzer (2004) pointed out that for porous media, water saturation is close to zero at the hot end of a heat pipe, which means that the "dry" thermal conductivity of the soil should be used for estimating energy transport in Equation (1). We will later demonstrate that this assumption does not hold for heat pipes in fractured porous media, where non-zero matrix saturations occur at the hot end of a heat pipe. Therefore, in contrast to the equations given in Birkholzer (2004), we have allowed for varying thermal conductivities λ_1 and λ_2 in Equation (1), to accommodate the possibility of this property changing with water saturation.

For transient heat pipes, the mass- and energy-balance equations include non-zero storage terms. Birkholzer (2004) suggested describing the migration characteristics of a transient

heat pipe by using a boiling front velocity $\dot{v}$, which can be easily determined from temperature profiles measured at different times. Using $\dot{v}$, the time derivatives in the storage terms were replaced with space derivatives, and the water flux q_L^T in a transient heat pipe was approximately derived by correcting the quasi-steady flux q_L^S as follows:

$$q_L^T \approx q_L^S + \bar{r}\dot{v}(1-\phi)\frac{\rho_S C_S (T_1 - T_2)}{r_2 \rho_L (h_G - h_L)} + \frac{\bar{r}\dot{v}\phi(S_{L,2} - S_{L,1})}{r_2}. \quad (2)$$

The first correction term in Equation (2) accounts for heating lower-temperature regions encountered by the migrating finite volume. Similar to Equation (1), this term contains site-specific quantities readily measured *in situ* or in laboratory experiments (e.g., average radius of the finite volume $\bar{r}$, boiling front velocity $\dot{v}$, porosity ϕ, grain density ρ_S, grain heat capacity C_S, temperatures T_1 and T_2) in addition to known thermodynamic properties of water and vapor. The second correction term, which accounts for the vaporization of resident pore water, contains liquid saturations $S_{L,1}$ and $S_{L,2}$ at both sides of the finite volume. Birkholzer (2004) pointed out that these saturations are not as easily obtained in the field as temperature data and therefore may not be available in given applications.

For systems with linear-geometry heat flow processes, the mass- and energy-balance equations were formulated independent of the distance from the heat source. Considering quasi-steady conditions, Birkholzer (2004) arrived at:

$$q_L^S \approx \frac{(\lambda_1 \nabla T_1 - \lambda_2 \nabla T_2)}{\rho_L (h_G - h_L)}. \quad (3)$$

For transient conditions, the quasi-steady flux were adjusted with flux correction terms as follows

$$q_L^T \approx q_L^S + \dot{v}(1-\phi)\frac{\rho_S C_S (T_1 - T_2)}{\rho_L (h_G - h_L)} + \dot{v}\phi(S_{L,2} - S_{L,1}). \quad (4)$$

As mentioned before, Birkholzer (2004) applied Equations (1) through (4) to various hypothetical test cases. The estimated water fluxes were in very good agreement with fluxes calculated from detailed simulation models for the respective cases, demonstrating the validity of the temperature-profile method. It was also observed that the transient corrections are often relatively small in porous media applications, and that the fluxes estimated under quasi-steady assumptions are reasonably approximations for the simulated fluxes.

3. Heat Pipes in Fractured Porous Rock

This section focuses on the specific characteristics of heat-driven flow processes in fractured porous formations, and the implications that these specific characteristics may have on the application of the temperature-profile method. We are specifically interested in conditions representative of the fractured tuff at Yucca Mountain, Nevada, the designated U.S. site for the geologic disposal of high-level radioactive waste.

3.1 The Intrinsic Heterogeneity of Fractured Porous Rock

In general, the thermal-hydrological processes in a fractured formation heated above boiling should be similar to those in a porous formation, with (1) vaporization of pore water and gas pressure buildup near the heat source, (2) vapor transport away from the heat source, (3) condensation in cooler regions, and (4) reflux of water towards the heat source, the latter influenced by capillarity and gravity (see brief discussion in Section 2.1). These processes are expected to be more complex, however, because of the intrinsic heterogeneity of the fractured porous rock at Yucca Mountain and the potential disequilibrium between the porous matrix and the rock fractures (Birkholzer and Tsang, 2000). The tuff matrix in the hydrogeological units hosting the repository has considerable porosity, but a very small permeability on the order of microdarcies or less. On the other hand, the formation is intensely fractured, with spacings of a few decimeters or less, and the continuum permeability of the fractures is many orders of magnitude larger than that of the rock matrix.

Since the fractures occupy only a very small volume fraction of the formation, the porous matrix stores the vast majority of the mass and energy in the system and accounts for most of the heat conduction. The potential for flow of liquid and gas, however, is limited. The highly permeable fracture network, on the other hand, has negligible storage capacity, but offers very effective conduits for gas and liquid flow, thereby generating significant convective heat transfer. Thus, global flow of liquid and gas will mostly occur in the fractures, while locally there will be mass exchange between the fractures and the matrix pores. Global transport of heat will occur by conduction in the matrix and by convection in the fractures, with conductive and convective exchange between them on a local scale. The mass and heat exchange between fractures and matrix is caused by a local temperature and pressure equilibrium, a result of the different response times to the thermal perturbation of the formation.

We may expect from this discussion that the evolution of heat pipes in a fractured porous formation will be affected by a complex interrelation between fracture and matrix flow and heat transport. Since heat pipes are driven by convective heat transfer from liquid-gas counterflow, the characteristics of heat pipes in fractured porous formations should mostly depend on the flow behavior in the fracture network. On the other hand, the energy consumed for the vaporization of water at the hot end of the heat pipe is provided by conductive transport in the porous matrix.

3.2 Simulated Heat Pipes Observed in a Hypothetical Example Case

For a more detailed analysis of the heat pipe behavior in fractured porous rock, we have conducted a numerical simulation of the thermal-hydrological conditions in a two-dimensional system that is a simplified version of the horizontal-tunnel emplacement design at Yucca Mountain. A heat source with a constant-strength line load is placed into a horizontal tunnel located in the center (x = 0 m and z = 0 m) of a vertical fractured-rock domain of 200 × 200 m^2 extent. The axis of the heater and the tunnel axis are orthogonal to the vertical domain. The tunnel radius is 2.75 m, identical to the future emplacement drifts planned at the Yucca Mountain repository. The selected heater power is 1,095 W/m, which corresponds to radioactive wastes approximately 12 years old. This heater power is identical to the average line load generated by the nine floor heaters in the Drift Scale Test, a large-scale underground heater test currently conducted at Yucca Mountain (Datta et al., 2004).

The hydrogeological and thermal properties of the formation surrounding the emplacement tunnel are given in Table 1. They are based on the property set developed for one of the hydrogeological units hosting the repository at Yucca Mountain—the Topopah Spring Middle Nonlithophysal Unit—close to the location of the Drift Scale Test (Birkholzer and Tsang, 2000). At ambient conditions, the matrix pores hold a significant amount of water owing to strong capillary forces, with saturation values of the order of 0.9. Assuming thermodynamic equilibrium with the matrix, the fractures are essentially drained of water, with saturation values close to residual saturation. Since the fractures are basically nonconductive at such small saturations and since the matrix has

such low permeability, the ambient percolation flux at Yucca Mountain is very small, i.e., a few millimeters per year. Prior to heating, the temperature in the domain is about 25°C, and the gas pressure represents the atmospheric pressure at the elevation of Yucca Mountain (about 0.89 bar).

The numerical simulator TOUGH2 (Pruess et al., 1999) was employed to determine the thermal-hydrological flow processes in the model domain after emplacement of heat-producing radioactive waste. The open tunnel was modeled as a gas-filled, zero-capillarity medium with a thermal conductivity of 10.6 W/(m-K). This large thermal conductivity approximates the radiative heat transfer that occurs between the heat source located in the center of the tunnel and the tunnel walls. The conceptual framework for simulating the intrinsic heterogeneity of the fractured porous formation was adopted from previous drift-scale models for Yucca Mountain (e.g., Buscheck et al., 2002; Haukwa et al., 2003; Birkholzer et al., 2004). In these models, the fractured rock is described using a dual-continuum concept, assuming two separate, but interacting continua that overlap each other in space, one describing flow and transport in the fracture network, the other describing flow and transport in the matrix (Doughty, 1999). A continuum representation of the fractures is appropriate because the fracture density is high, and a well-connected fracture network forms at the scale of interest. Global flow and transport occur within both the fracture continuum and the matrix continuum, while local fracture-matrix interaction occurs between the two continua as a result of local pressure and temperature differences.

Figure 2 gives a close-up view of the simulated thermal-hydrological conditions—matrix temperature, liquid saturation and flux in matrix and fractures—in the vicinity of the emplacement tunnel after 4 years of heating. At this time, the near-field rock has heated up considerably to maximum temperatures of more than 150°C (Figure 2a), and a dry conduction-dominated zone has evolved in the fractured formation extending a few meters away from the tunnel (Figures 2b and 2c). The initially stagnant pore water in the matrix becomes mobile through boiling. Since the matrix permeability is small, the produced vapor moves into the neighboring fractures as the permeable conduits and then migrates away into cooler regions. Subsequent condensation generates a zone of elevated water saturation and strong flux perturbation in the fractures just outside of the dryout zone, as is evident from Figure 2c.

While the temperature field appears radial-symmetric—as the heat transfer is conduction-dominated—the saturation and flux fields show distinct differences between the regions above and below the heat source. These differences result from gravitational forces. Vapor that condenses in the fractures above the heat source is mostly driven back to the boiling zone by the combined impact of capillarity and gravity (Figure 2c). In contrast, condensate below the heater is exposed to counteracting forces as capillarity pulls upward and gravity pulls downward. While there is a net upward flow of water just below the boiling front (because of capillary forces dominating gravity forces), a considerable fraction of the condensate drains off away from the tunnel. Along the way, some fraction of the condensate flowing in the fractures also imbibes into the matrix, a result of local capillary barrier differences, and becomes largely immobile again. For example,

imbibition of fracture-water into the matrix pores creates a zone of elevated matrix saturation below the tunnel (Figure 2b). Altogether, the flux perturbation in the matrix is much less significant than in the fractures, as indicated by the almost invisible flux vectors.

Figures 3 and 4 show simulation results after 4 years of heating in the form of temperature, saturation, gas pressure, and flux profiles, the first profile vertically up from the tunnel crown, the second profile vertically down from the tunnel floor (see Figure 2a for the location of the boreholes). The plotted curves distinguish between the matrix and the fracture continuum. Note that the temperatures in fractures and matrix are virtually identical, indicating that the local heat exchange is strong enough to force a rapid equilibrium as thermal perturbation occurs. This finding is typical in densely fractured formations such as the fractured tuff at Yucca Mountain, where small fracture spacings generate a large interfacial area for energy exchange (Doughty, 1999). That a local thermal equilibrium cannot be generally expected in fractured porous formations is demonstrated later in this paper, when a sensitivity case with lower fracture density is presented (Section 4). Both temperature profiles in Figures 3 and 4 show distinct heat-pipe signatures, evidenced by the difference in gradients and the extent of the nearly isothermal zone.

For further analysis, we plotted the finite volumes that need to be defined for the temperature gradient method at the hot end of each heat pipe, i.e., at the interface between the inner conduction zone and the heat-pipe region. Interestingly, this location

coincides with an almost-zero saturation in the fractures, suggesting that all refluxing water boils off (behavior similar to porous media heat pipes), but shows considerable matrix saturations between about 0.5 and 0.9. In fact, a significant portion of the inner conduction zone with temperatures clearly above the nominal boiling point of water remains at non-zero matrix saturation. The reason for this behavior becomes evident in the pressure profiles (Figures 3b and 4b). While the gas pressure in the fractures is hardly affected by boiling (since vapor can effectively move away in the fractures), there is a strong pressurization in the matrix with maximum pressures between 1.3 and 1.4 bars, a result of the small matrix permeability limiting the vapor release from the matrix pores. As the pressure builds up, the boiling point of water increases, allowing for the presence of liquid water in the matrix despite rock temperatures that are well above 100°C.

The simulated fracture and matrix flux profiles are depicted in Figures 3c and 4c, together with the combined flux derived by adding the fracture and matrix flow components. For better comparison of the heat-pipe intensity, fluxes are plotted following the convention that positive values indicate flow away from the heat source and negative values indicate flow towards the heat source. (Thus, negative fluxes above the heater flow downwards; negative fluxes below the heater flow upward). The larger reflux occurs above the heater, where capillarity and gravity create a maximum downward flux of about -300 mm/yr (combined flux in fractures and matrix). The reflux below the heater is smaller, at about -200 mm/yr, where gravity works against capillarity. The differences in the reflux magnitude are clearly reflected in the temperature profiles, with the heat-pipe signatures stronger for the vertical profile above the tunnel. Of the maximum combined

reflux, about 80 to 90% are contributed by fracture flow; the remaining 10 to 20% are contributed by the matrix. That the matrix flux contribution is not negligible—despite the orders of magnitude smaller permeability compared to the fractures—is a result of the large capillary strength in the matrix, and the corresponding capillary pressure difference at the hot end of the heat pipe.

3.3 Implications for Temperature-Profile Method

The fact that the thermal-hydrological conditions in a fractured porous formation may be in local disequilibrium raises some interesting questions regarding the analysis of heat pipe fluxes with the temperature-gradient method. The first question is whether the local matrix or the local fracture conditions should be used in the temperature-profile calculations. Theoretical considerations may give the answer: We would expect that the temperatures and saturations need to be representative of the matrix conditions because (1) the conductive transport of heat in Equations (1) or (3) occurs almost entirely in the matrix, and (2) because the mass and energy storage described in Equations (2) or (4) occurs almost entirely in the matrix.

A related question is whether the data presumably to be used for the temperature-profile method—i.e., those representing the thermal-hydrological behavior in the matrix—would be consistent with the parameters typically measured in the field. One can safely assume that all grouted temperature sensors yield measurements representative of matrix conditions. Also, *in situ* measurements of saturation will typically give the moisture

content in the matrix, since the majority of the storage capacity in the formation is provided by matrix pores.

The final question is how accurate the temperature-gradient method can be in cases with local disequilibrium between the matrix and the fractures. The measured temperatures—representative of the matrix conditions—may not fully capture the heat-pipe fluxes that mostly occur in the fracture network. As seen in Section 3.2, the total reflux in a heat pipe is composed of fracture and matrix contributions. Thus, for good accuracy, the estimated fluxes derived from the temperature-gradient method must represent the total reflux in the fractures and the matrix blocks.

Other important implications for the application of the temperature-profile method stem from the observed matrix saturation results (see Figures 3 and 4). Since the hot end of the heat pipe is not at zero saturation, as is generally the case in porous media, we need to account for saturation-dependent thermal-conductivity values in Equations (1) and (3). We can also expect that the saturation-dependent flux-correction terms in the transient Equations (2) and (4) will be more relevant for the flux estimation than in porous media applications. It follows that knowledge of the matrix saturation at the hot end of heat pipes is important when applying the temperature-profile method to fractured porous formations.

4. Testing the Temperature-Profile Method for Fractured Porous Media

We test the accuracy of the temperature-profile method for fractured media by applying it to the example problem discussed in the Section 3.2. Let us assume that the simulated matrix temperature and matrix saturation profiles depicted in Figures 3 and 4 are measured data from a field application. The nodal points of the finite volume discretization may represent temperature sensors distributed along vertical "boreholes". (Note, however, that the presence of these boreholes was not actually modeled in the simulation runs.) The saturation values may have been estimated from geophysical methods or from core analysis. We furthermore assume that the saturation-dependent thermal conductivity of the rock matrix (as well as other necessary rock properties such as grain heat capacity, grain density, and porosity used in the example problem) has been determined from field or laboratory measurements (see Table 1). We can then apply Equations (1) and (2) to determine the approximate liquid fluxes at quasi-steady and transient conditions. We use Equations (1) and (2) instead of Equations (3) and (4) because the considered temperature fields in this example case are radial-symmetric in nature. We finally compare the approximate fluxes to the simulated fluxes given by the numerical model. Good agreement between the approximate and the simulated fluxes would suggest that the temperature-profile method works for the specific conditions in fractured porous formations.

As pointed out in Birkholzer (2004), the starting point of the temperature-profile method is a thorough analysis of the temperature profiles to determine the heat-pipe

characteristics in the system. A valuable practice in this regard is to determine the gradients between two adjacent sensors (nodal points) and to plot these together with the temperature profile. Plotting the gradients for the example problem clearly reveals the presence of heat pipes at the selected time (t = 4 years after heating starts) in both considered boreholes (Figure 5), manifested in strong gradient changes within a short distance at radii $r \approx 6$ m (borehole vertically up) and $r \approx 6.5$ m (borehole vertically down), respectively. For comparison, we have depicted both matrix and fracture results, with only minor differences between the matrix and fracture gradients close to the heat pipe region.

Based on the discussion in Section 3.3, we use the matrix temperature data for the temperature-profile method, and choose finite volumes with appropriate radii r_1 and r_2 near the hot end of the heat pipe. Radius r_1 should be safely located in the inner conduction zone, with gradient changes related only to the radial geometry of the conductive heat flow processes. Radius r_2 should be safely located in the heat pipe region, where the temperature gradients are small and remain almost uniform with increasing distance from the heat source (Birkholzer, 2004). For both radii, we obtain the necessary matrix data values—temperature gradients ∇T_1 and ∇T_2, temperatures T_1 and T_2, saturations $S_{L,1}$, and $S_{L,2}$—from the simulation results. The saturation-dependent thermal conductivities λ_1 and λ_2 can then be interpolated from the determined saturations using the well-established square-root interpolation formula given in Table 1. The interpolation is based on the known thermal conductivities at oven-dried conditions (dry thermal conductivity) and at full water saturation of the sample (wet thermal

conductivity). With given radii, temperature gradients, and thermal conductivity values, we can use Equation (1) to determine the liquid fluxes in the heat pipe under quasi-steady assumptions.

For the transient calculation according to Equation (2), we also need to determine the boiling front velocity at the considered time step *t*. Following Birkholzer (2004), we use two additional temperature profiles measured at times $t_a = t - \Delta t$ and $t_b = t + \Delta t$. The next steps are to determine the boiling point locations *r*, r_a, and r_b at times *t*, t_a, and t_b (i.e., the locations of the hot end of each heat pipe), to obtain the differences $\Delta r_a = r - r_a$ and $\Delta r_b = r_b - r$ between these locations, and to calculate two boiling front velocities $\dot{v}_a = \Delta r_a / \Delta t$ and $\dot{v}_b = \Delta r_b / \Delta t$. The resulting boiling front velocity $\dot{v}$ at time *t* is then derived as the arithmetic average of the two values $\dot{v}_a$ and $\dot{v}_b$. With given velocity, temperature, and saturation values, we can finally apply Equation (2) for the transient heat pipe fluxes.

Figure 6 compares the liquid fluxes obtained from the temperature-profile method with those from the simulation model. (Additional details on the flux calculations are given in Table A1 in Appendix A.) Results are presented for the temperature profiles given in Figure 5 (at $t = 4$ years) as well as for two additional times at $t = 2$ years and $t = 8$ years. The simulated fluxes in Figure 6—plotted as dashed lines—show the combined reflux in the fractures and the matrix. The agreement between these simulated fluxes and the flux results calculated from the transient heat pipe solution are excellent, for both boreholes and all three times. The temperature-profile method appears to work well for heat pipes

in fractured porous formations, at least for an application in which the saturation-dependent thermal conductivities can be determined because saturation measurements are available.

The error bars in Figure 6 demonstrate the possible range of results when using the dry and the wet thermal conductivity for the flux evaluation, as may be necessary when the exact nature of the saturation dependence of thermal conductivity is not known in a given application. The smaller dry thermal conductivity of 1.67 W/m-K results in fluxes that are smaller in magnitude (less negative); the larger wet thermal conductivity gives fluxes larger in magnitude (more negative). The uncertainty range introduced by the possible range of thermal conductivity values is reasonably small, with up to 20% of the flux estimates.

Figure 6 also gives the flux estimates calculated from the quasi-steady heat-pipe solution (hollow symbols). These fluxes are consistently larger in magnitude (more negative) than the simulated results, indicating that a noticeable fraction of the energy is used for heating the system and vaporizing pore water as the heat pipe migrates. As pointed out in Birkholzer (2004), the quasi-steady fluxes provide valuable upper-bound estimates for the correct transient results in porous media applications with unknown heat-pipe saturations, in which the transient corrections cannot be determined. This seems similarly possible in the considered fractured media example, since the difference between the quasi-steady results and the simulated fluxes is generally not larger than about 15%. However, knowledge of water saturation at the hot end of the heat pipe is also necessary

for the determining thermal conductivity. In other words, without measured saturation values, or at least reasonable estimates of saturation at the hot end of the heat pipe, the flux estimates would carry a combined uncertainty from the unknown transient correction and from the unknown saturation-dependent thermal conductivity.

It was observed earlier in this paper that the simulated temperatures in the matrix and the fracture continua are virtually identical for the considered example. To thoroughly test the temperature-profile method, we need to study another sensitivity case with disequilibrium conditions. Therefore, we have slightly revised the above-considered example by using a ten-times-smaller interfacial area between the fractures and the matrix. A smaller interface area would be related to a change in the fracture-network geometry, such as having a less dense fracture population. All other properties, as well as the initial and boundary conditions, are identical to the base case. Figure 7 gives selected simulation results for this revised case in the form of temperature profiles and temperature gradients along the two vertical boreholes at 4 years of heating. While in perfect agreement outside of the heat pipe region, there are significant differences between the matrix and fracture temperatures within and at both ends of the heat pipe. It appears that the mostly conductive local transfer of heat from the matrix to the water/vapor phases in the fractures is not intense enough to balance the temperature changes invoked by the strong convective energy transport in the fracture continuum. As a result, drastic gradient changes occur in the fractures. At the hot end of the heat pipe, for example, the change in the matrix gradients is about 5-15 °C/m, in contrast to the change in the fracture gradients of about 20-30 °C/m. Consequently, application of the

temperature-profile method would lead to strongly different results when using the fracture instead of the matrix gradients.

We conducted the temperature-profile analysis for the revised simulation case, following the procedure applied in the base case. Specifically, we used the matrix temperature and saturation data for the calculation of fluxes, as suggested earlier in this paper. Figure 8 gives the flux estimates derived from this approach compared to the simulated fluxes, showing very good agreement between the estimated transient fluxes and the simulated results (see also Table A2 in Appendix A for more detailed information). This clearly confirms that the temperature-profile method can be applied to fractured formations even for disequilibrium conditions, and that the temperature gradients to be used for the analysis are those representative of the matrix thermal behavior. Note that the heat-pipe fluxes obtained for this revised simulation case are considerably smaller than those of the base case (compare with Figure 6). Because of the reduced fracture/matrix interface area, there is more resistance for the produced vapor to escape from the matrix pores into the fracture system, leading to a stronger gas pressure increase. As a result, the boiling temperature in the matrix rises, and vapor is generated at a lesser rate, thereby reducing the heat-pipe intensity.

5. Analysis of Temperature Data from the Yucca Mountain Drift Scale Test

To demonstrate its potential in field studies, we apply the temperature-profile method to data from a large-scale underground heater test performed in the fractured tuff rock at the geologic repository for nuclear waste at Yucca Mountain, Nevada. The so-called Drift Scale Test (DST) is currently being conducted to probe the coupled thermal, hydrological, mechanical, and chemical processes likely to occur in the unsaturated rock mass around the geologic repository (Datta et al., 2004). For this illustrative example, we select a subset of the approximately 1,750 temperature sensors in the DST and estimate the magnitude of the flux perturbation along vertical boreholes drilled into the heated fractured tuff.

5.1 Configuration of the Drift Scale Test

The DST test site is located in a side alcove of an underground tunnel, the Exploratory Studies Facility (ESF), at a depth of about 250 m in the densely fractured tuff of the Topopah Spring Middle Nonlithophysal Unit (Birkholzer and Tsang, 2000). The DST centers around a horizontal tunnel segment ("heated drift"), which is 5 m in diameter and about 50 m long (Figure 9). The heated drift is separated from the access tunnels by a thermal bulkhead, which is a good insulator to heat, but relatively open to gas transport. Heating is provided by nine floor heaters placed along the heated drift, as well as by 50 rod heaters, referred to as "wing heaters," which are placed into horizontal boreholes emanating from and orthogonal to the heated drift. The dimensions of the heated drift and the dimensions of the floor heaters are similar to the current design of waste emplacement

drifts at Yucca Mountain. The heaters of the DST were activated on December 3, 1997, with a combined maximum power of about 190 kW, about one third of which was provided by the floor heaters. The heating phase continued for approximately four years, until January 14, 2002, when heater power was turned off. Our analysis focuses on the heating phase of the test. Currently, the DST is in the midst of a four-year period of natural cooling.

Detailed site characterization with field and laboratory analysis conducted prior to heating provided relevant hydrological and thermal properties of the fractured rock in the DST, as given in Table 1. For monitoring purposes, the DST test block was instrumented with thousands of sensors to collect thermal, mechanical, hydrological, and chemical data during the test duration (Datta et al., 2004). Radial clusters of 20 m long boreholes emanating from the heated drift monitor the temperature evolution, as do longitudinal boreholes parallel to the heated drift (Figure 9a). The radial clusters comprise between 2 and 8 boreholes arranged in vertical cross sections orthogonal to the drift axis (see one of the clusters depicted in Figure 9b). Resistance temperature devices (RTDs) were installed and grouted at approximately 30 cm intervals in each of these boreholes, with individual data produced on at least an hourly basis. This temporal and spatial resolution provides an excellent data support for analyzing the heat pipe behavior in the fractured formation.

Water saturation in the tuff matrix was measured with geophysical techniques, such as ground penetrating radar (GPR), electrical resistivity tomography (ERT), and neutron logging (Bechtel SAIC Company, 2004b). For the purpose of determining water

saturation at the hot end of heat pipes, the neutron logging data are most valuable because they provide quantitative data on a local scale. (The rock volume covered by neutron logging is approximately 10 to 15 cm from the borehole.) GPR and ERT techniques, on the other hand, cover much larger portions of rock, and results are typically more suited for qualitative rather than quantitative analysis. Two longitudinal boreholes parallel to the heated drift were equipped with neutron tubes that had RTD bundles attached on the outside and were grouted in place. Neutron logging measurements were conducted every few months throughout the heating phase of the test.

5.2 Thermal-Hydrological Processes in the DST

The coupled processes occurring in response to heating in the DST have been evaluated in various scientific studies, focusing on hydrological perturbations (e.g., Birkholzer and Tsang, 2000; Mukhopadhyay and Tsang, 2003), mechanical perturbations (e.g., Rutqvist et al., 2004), and chemical perturbations (e.g., Sonnenthal et al., 2004). In principle, the ambient hydrological situation as well as the thermal response of the DST are similar to the two-dimensional example case discussed in Section 3. Prior to heating, the DST had fairly uniform conditions with rock temperature at about 24°C, gas pressure at about 0.89 bar, saturation in the porous rock matrix at about 0.9, and saturation in the fractures close to the residual value. Despite the relatively high saturation in the matrix, the overall percolation flux arriving at the test location was almost negligible at a few millimeters per year, a result of the very small permeability of the rock matrix. After the heaters were turned on, the rock temperatures near the drift wall and close the wing heaters increased to the boiling point of water within less than a year (Birkholzer and Tsang, 2000). The

maximum temperatures observed in the fractured porous rock were about 200°C near the drift wall and more than 250°C in some sensors close to the wing heaters.

The temperature-profile method requires the heat-transfer processes to be approximately one-dimensional, either radial-symmetric or linear. In the DST, the temperature changes measured along the drift axis were in general much smaller than temperature changes perpendicular to the drift, as demonstrated by the similarity between temperature profiles obtained in radial clusters at different distances from the bulkhead. Therefore, the resulting temperature field can be evaluated using two-dimensional cross sections perpendicular to the drift axis. Within these two-dimensional cross sections, however, the temperature contours have both radial and linear features because of the complex DST heater geometry, with the in-drift floor heaters creating a radial temperature field and the horizontal wing heaters creating a linear temperature field.

To better understand which geometry assumption is better suited, we can take a closer look at the measured temperature field. Figure 9b shows the location of the 95°C-isotherm in a representative two-dimensional cross section at different times of heating, as interpolated from the radial borehole temperatures (Bechtel SAIC Company, 2004b). (Note that the boiling temperature is about 96°C at the elevation of Yucca Mountain.) The strongly asymmetrical shape of the isotherms indicates that the heat-transfer processes along the vertical boreholes are more linear than radial. We will therefore apply the linear heat-pipe solution as the most likely case, but will present radial heat-pipe calculations for comparison.

5.3 Analysis of Temperature Profiles

Figure 10 shows the measured temperature profiles from two selected vertical boreholes, one drilled from the heated drift vertically up (Borehole 137), the other drilled from the heated drift vertically down (Borehole 141). Circular symbols indicate the location of temperature sensors. Both boreholes are located at a distance of about 12 m from the bulkhead end of the heated drift; their geometry is similar to the eight-borehole cluster depicted in Figure 9b. The profiles in Figure 10 show the temperature conditions after 2, 3, and 4 years of heating. Analysis of an earlier time step at 1 year was dismissed because distinct heat pipes had not yet developed—in part because preheat evaporative drying in the vicinity of the open drift had decreased the water content available for boiling and recirculation processes, in part because the maximum temperatures measured along the boreholes had just risen above the boiling point of water.

For the considered times, above-boiling conditions extend from the drift wall (at 2.5 m from the drift center) up to several meters into the fractured tuff (Figure 10). The maximum temperatures are generally higher above the drift (Borehole 137) than below (Borehole 141). This difference is mainly caused by a concrete invert of about 1.2 m maximum thickness that was constructed to provide a flat drift floor. The invert shields the fractured rock from direct thermal radiation by the nine floor heaters and thus retards the temperature buildup measured in the lower borehole. Heat-pipe signatures are evident in both boreholes at all depicted times. Similar to the results obtained in Section 4, the heat pipes above the heater appear stronger than the ones below the heater, indicating enhanced reflux because of gravitational forces working together with capillary forces.

This assessment is confirmed by the temperature gradients that have been calculated and plotted using data from adjacent sensors (green line with square symbols). The magnitude of the upper gradients in the inner conduction zone is significantly larger (more negative) in Borehole 137, and so are the differences between the upper gradient and the gradient measured within the heat-pipe zone. As pointed out before, these gradient differences are directly linked to the amount of liquid reflux occurring in a heat pipe.

For application of the temperature gradient method, we visually define the "best" finite volumes for each heat pipe in Figure 10, illustrated as shaded areas. While the measured temperature profiles appear very smooth—a result of the forgiving nature of heat conduction—the gradient profiles show data noise, which makes the determination of finite volume location (as expressed by the distance from the heat source, r_1 and r_2) and the choice of gradients (∇T_1 and ∇T_2) somewhat subjective and arbitrary. As Figure 10 suggests, the smaller gradients, ∇T_2, are usually less problematic, with relatively small gradient changes within the heat pipe region. On the other hand, the upper gradients, ∇T_1, expose considerable zigzag behavior, possibly caused by measurement inaccuracies and small-scale heterogeneities. In such cases, the resulting flux estimates would be strongly affected by the subjective selection of location r_1 and upper gradient ∇T_1.

To evaluate the uncertainty introduced by data noise, we generally recommend using more than one location r_1 and gradient ∇T_1 for the calculation of fluxes. The locations r_1 of each profile in Figure 10, for example, have been defined by choosing the first upper gradient that is clearly outside of the change-of-gradient region at the hot end of the heat-

pipe zone. However, the temperature-profile method is not only applied to this location and gradient, but also to the next four locations and gradients in the upstream direction, and the average flux is then used as the "best-estimate" result. The range of fluxes covered by the individual flux estimates indicates the uncertainty of the temperature-profile method.

As can be seen from the location of the finite volumes, the heat pipes depicted in Figure 10 migrate away from the heat source with time, more so above the heated drift than below. We evaluate the migration characteristics of the heat pipes at the depicted times by determining the boiling front velocities, following the procedure described in Section 4. We use a $\Delta t = 0.25$ years, meaning that, for example, the approximate progress of the boiling front at t = 3 years is evaluated from additional temperature measurements at times $t_a = 2.75$ years and $t_b = 3.25$ years. Velocities range from about 1.3 (at 2 years) to about 0.8 m/yr (at 4 years) in Borehole 137, compared with about 2.2 to about 0.9 m/yr in Borehole 141. The initially faster boiling front propagation in Borehole 141 is a result of less intense recirculation of vapor and water below the heater.

As discussed above, the temperature contours measured in a two-dimensional cross section orthogonal to the drift axis have ellipsoidal shape; i.e., they may have both radial and linear features. Analysis of the temperature gradients can further help to identify the geometrical nature of heat transport along a borehole. Both vertical boreholes are directed approximately parallel to the direction of the main heat flow, as the temperature-profile method requires; the slight horizontal offset (≈ 0.75 m) of the two boreholes from the

center of the drift (see Figure 9b) can be neglected. Borehole 141 features temperature gradients in the inner conduction zone that are fairly uniform, independent of the distance from the drift center. Thus, the conductive heat-transfer processes below the heater are predominantly linear. In contrast, for Borehole 137, the temperature gradients in the inner conduction zone vary with increasing distance from the drift center (radius). It appears that the conductive heat-transfer processes above the heater have some radial component. The differences in the conductive behavior above and below the drift are caused by two effects: (1) the horizontal wing heaters are located about 0.6 m below the centerline of the drift, thus conducting more linear energy into the lower part of the DST, and (2) the concrete invert at the bottom of the drift shields the lower part of the DST from some fraction of the radial energy supplied by the floor heaters.

5.4 Analysis of Saturation Measurements

As pointed out in Section 3.3, knowledge of matrix water saturation at the hot end of the heat pipe is important when applying the temperature-profile method to fractured porous formations. Since saturation was not measured in the radial boreholes selected for our analysis, we employ data from other boreholes equipped with combined RTD and neutron logging devices to establish a temperature-saturation relationship for the relevant temperature range. The two boreholes equipped with such combined devices are the horizontal Boreholes 79 and 80 (see Figure 9a). The boreholes run along the full length of the heated drift at a distance of a few meters from the heat sources.

In Figure 11, we have plotted the saturation-temperature data points from all sensors and measurement times for Borehole 79. Owing to gas pressure buildup in the matrix, liquid

water is present at temperatures well above 96°C. Despite some data scatter, the general trend of matrix saturation as a function of temperature is the same over all data points, particularly over the temperature range relevant in this analysis (i.e., the temperatures measured at the hot end of the heat pipe). Similar results can be seen from Borehole 80. We may therefore assume that the saturation-temperature relationship depicted in Borehole 79 also holds for the selected radial boreholes. Using this relationship, we can easily derive saturation values $S_{L,1}$ and $S_{L,2}$ from the measured temperatures T_1 and T_2 at the hot end of each heat pipe depicted in Figure 10. To facilitate the interpolation, we have derived an interpolation function from all data points using a standard smoothing algorithm (see the heavy black line in Figure 11). Once the saturation values have been determined, the saturation-dependent thermal conductivity values λ_1 and λ_2 can be calculated using the formula given in Table 1.

5.5 Flux Estimates from the Temperature-Profile Method

Using temperatures and temperature gradients at both sides of the finite volumes shown in Figure 10, the corresponding saturation and thermal conductivity values as derived above, and the relevant rock matrix properties given in Table 1 (grain heat capacity, grain density, and porosity), we can finally apply Equations (1) through (4) to calculate the heat-driven liquid fluxes in the DST. The best flux estimates are those calculated with the transient heat-pipe solution assuming linear geometry, using Equation (4). However, for the sake of comparison, we have also looked at quasi-steady estimates and at the radial-geometry case.

Figure 12 shows the heat-pipe flux results for Borehole 137 (Figure 12a) and Borehole 141 (Figure 12b) as a function of time. The solid square symbols give the transient fluxes averaged over five upstream locations and gradients for the linear case. Again, the convention is that negative flux values denote flow towards the heat source. For Borehole 137, the average fluxes assuming linear geometry are about -470 mm/yr at 2 years, about -430 mm/yr at 3 years, and about -340 mm/yr at 4 years. These fluxes are much stronger than the ambient percolation fluxes of a few millimeters per year at Yucca Mountain, which confirms model predictions stating that the decay heat to be emplaced at Yucca Mountain will generate significant flux perturbation in the near-field fractured rock (Bechtel SAIC Company, 2004a).

Similar to the results obtained in Section 4, the heat-pipe fluxes measured below the heater are smaller than the ones above. The average transient fluxes in Borehole 141 range from about 140 mm/yr to about 230 mm/yr, assuming linear geometry. That the fluxes in Borehole 141 are smaller than those in Borehole 137 confirms that much of the condensate produced below the heater drains away from the heated area as a result of gravity, a process quite important for the performance of the future repository (Bechtel SAIC Company, 2004a). In contrast to Borehole 137, the transient fluxes in Borehole 141 increase with time between 2 and 3 years of heating. This may be a result of the region below the tunnel being sheltered by the concrete invert, which appears to retard the temperature perturbation at early times. Another possible reason is the heterogeneity of the fractured porous rock. The heat-pipe location at two years could possibly be located in a low-permeability region, which would reduce the flux intensity.

The error bars in Figure 12 give an indication of the uncertainty range of the flux estimates stemming from the variability of the five upstream temperature gradients. This variability may be a result of measurement errors (data noise, sensor resolution) or may be caused by the small-scale heterogeneity of the fractured rock. On average over all times, the flux uncertainty displayed by the error bars is about 100 mm/yr, which translates into approximately 25% of the average fluxes for Borehole 137 and about 50% of the average fluxes in Borehole 141. This level of accuracy is reasonably good for any kind of field data, but is in this instance particularly impressive considering that there is no direct method for measuring underground fluxes in the field.

Another potential source of uncertainty in applying the temperature-profile method stems from the complex heat-transfer geometry in the DST. The flux estimates in Borehole 137, for example, would be about 25 to 30% smaller assuming that the heat-transfer processes above the heater were radial and not linear (see the solid diamonds in Figure 12). Thus, the range of possible fluxes estimated from the temperature-profile method would be quite broad without knowledge about the geometry of the heat transfer processes. However, as shown above, additional analyses of temperature data can help to determine whether radial or linear processes dominate along a borehole, which makes one of the flux estimates more probable than the other. One should also point out that the complex geometry of the DST is rather unusual. Most applications, such as the emplacement of heat-generating waste at Yucca Mountain, have rather simple geometries that can be easily categorized into an either radial or linear heat transfer behavior.

Let us also evaluate the importance of the transient component in the estimated fluxes. For comparison with the transient results, flux estimates from the quasi-steady heat-pipe solution are depicted as hollow symbols in Figure 12. The quasi-steady results are not very accurate; they are much larger in magnitude (more negative) than the transient fluxes. This is particularly true for Borehole 141 below the heated drift, where the migration of the boiling front is faster than above. The transient flux corrections, i.e., the differences between the quasi-steady and the transient fluxes, range from about 70 up to 200 mm/yr. Such differences are significant, even in light of the various uncertainties in the flux estimates, and should not be disregarded. It follows that heat pipes in fractured media, with a thermal perturbation as intense as in the DST, should not be treated as a stationary system in a temperature-profile analysis. Closer evaluation reveals that the main contributor to the transient flux correction is the saturation-dependent term in Equations (2) and (4), i.e., the term that accounts for the vaporization of resident pore water as the boiling front migrates. Thus, in cases where a transient heat-pipe solution is necessary, knowledge of water saturation at the hot end of the heat pipe is an essential prerequisite for the application of the temperature-profile analysis. To establish whether the transient flux results are affected by the choice of data used for deriving the saturation-temperature relationship, we have conducted two separate flux calculations using neutron logging measurements from Borehole 79 (see Figure 11) and Borehole 80 (not depicted in this paper). The differences are marginal, on the order of less than 10 mm/yr.

Our final goal is to evaluate the impact of intermediate-scale flux heterogeneity in the DST block, using results from the temperature-profile analysis. We define intermediate-scale heterogeneity in the context of this paper as heterogeneity occurring on a scale of, say, 5 to 10 m. In particular, we like to analyze whether the heat-driven fluxes are strongly variable when measured at different borehole locations along the heated drift. For this purpose, we conduct a temperature-profile analysis for additional vertical boreholes from two other radial borehole clusters in the DST. We choose Boreholes 158 and 162 located at a distance of about 23 m from the bulkhead of the heated drift, as well as Boreholes 170 and 173 located at a distance of about 39 m from the bulkhead of the heated drift. The geometry of these boreholes is virtually identical to the radial cluster that includes Boreholes 137 and 141 (see Figure 9b). With such similarity in geometry and heat input between the three spatial clusters, the thermally perturbed fluxes in the additional boreholes should be fairly close to those derived for Boreholes 137 and 141; major differences can be directly attributed to the intermediate-scale variability of the thermal-hydrological properties. We have analyzed the heat-pipe signatures in the additional boreholes (see example graphs of temperature profiles for all six boreholes in Figure 13), conducted a temperature-profile analysis for each borehole at 2, 3, and 4 years of heating, and plotted the resulting fluxes in Figure 14a (for all boreholes oriented vertically up) and Figure 14b (for all boreholes oriented vertically down).

Both the temperature profiles and the flux results indicate strong variability among boreholes that have similar geometry, suggesting that there is considerable heterogeneity within the fractured porous formation. The flux magnitude in Borehole 158, for example,

is about 200 to 300 mm/yr (or up to 60%) smaller than that in the comparable Borehole 137 (Figure 14a). This small flux correlates with the fact that the heat-pipe signatures in Borehole 158 are not very distinct, to the extent that no heat-pipe analysis was possible at 2 years of heating. Borehole 158 is apparently located in a zone where thermal-hydrological properties limit the magnitude of heat-pipe processes, possibly a zone with very small fracture permeability. Boreholes 137 and 170, on the other hand, show similar heat-pipe signatures in Figure 13, and the flux estimates follow roughly the same temporal trend, with differences on the order of about 20%. Comparable heterogeneity can be seen below the drift. Here, Boreholes 141 and 162 feature similar heat-pipe behavior and yield similar flux estimates, while Borehole 173 behaves differently. The larger flux estimates for Borehole 173 (Figure 14b) correlate well with the stronger heat-pipe signature in Figure 13, which is evident from the large gradient change and the extended temperature plateau. Note also that the location of the heat-pipe zone in Borehole 173 is much closer to the heat source than in the other two boreholes, suggesting that the migration of the boiling front has been slowed down by intense re-circulation of vapor and water. That the estimated fluxes are consistent with characteristic temperature signatures suggests that a detailed visual comparison of temperature profiles from different boreholes may already provide useful qualitative information on the flux heterogeneity.

6. Summary and Conclusions

A temperature-profile method was applied to evaluate the magnitude of the thermal perturbation in superheated fractured formations, where strong heat-driven fluxes may occur in geologic heat pipes. Heat pipes form when the vaporization and subsequent condensation of pore water create a continuous recirculation of water and vapor in the vicinity of the heat source. The general approach in this paper is to use high-resolution temperature data to derive the amount of energy consumed for water vaporization, which can then be used to calculate the amount of reflux. The information necessary for the application of this method includes temperature profile characteristics (i.e., the temperatures and temperature gradients at the hot end of the heat pipe as well as the migration velocity of the boiling front), thermal properties of the formation, saturation measurements, and a general idea of the heat transfer geometry.

The temperature-profile method was originally presented for porous media applications (Birkholzer, 2004). Since the thermal-hydrological processes in fractured porous rock are much more complex than in porous media—a result of the matrix rock and the fractures acting very differently in response to heating—we have first tested the applicability of the temperature-profile method in comparison with a dual-continuum model simulation for a hypothetical fractured system. We calculated water fluxes from the temperature-profile method using the simulated temperature profiles and saturation results, and compared them with the simulated fluxes. In a second step, we applied the temperature-profile method to measured data from the Drift Scale Test (DST), a large-scale underground heater test currently conducted in the fractured tuff formations at Yucca Mountain.

In fractured porous formations, the porous low-permeable matrix is mostly accountable for the heat-conduction processes, and also provides the vast majority of the storage capacity for mass and heat. The highly permeable fractures, on the other hand, act as effective conduits for vapor and water movement, thereby allowing for significant convective transport. Because of these differences, thermal perturbations often create strong local disequilibrium between the fractures and the matrix, with respect to the hydrological as well as the thermal conditions. Since heat pipes are driven by convective heat transfer, the characteristics of heat pipes in fractured porous formations—e.g., the location and the extent of the heat pipe—are strongly affected by the flow behavior in the fracture network. On the other hand, the energy provided for the vaporization of water is determined by the conductive transport in the porous matrix.

Despite these complexities, the temperature-profile method was shown to give flux estimates that compared very well with the simulation results in the hypothetical example. The estimated fluxes accurately reproduced the combined maximum reflux occurring in the fractures and the porous matrix, even for conditions with strong local temperature differences between the two media. It is important, though, that the measured temperatures used in the analysis be representative of the thermal-hydrological response in the porous matrix, meaning that the temperatures sensors should be grouted into boreholes. Data from open boreholes would most likely provide temperature profiles that would not reflect the conductive behavior in the matrix, thus overestimating the energy provided for boiling of water.

Applying the temperature-profile method to fractured porous formations also requires some knowledge of the matrix saturations at the hot end of the heat pipe. Despite temperatures well over the nominal boiling point at atmospheric conditions, water can be present in the matrix pores because of gas pressure buildup in response to vapor production. This water presence needs to be accounted for in the storage terms of the heat-pipe solutions, and it also affects the magnitude of thermal conductivity values to be used in the flux calculation.

Application of the temperature-profile analysis to data from the large-scale *in situ* heater test (DST) demonstrated the general feasibility of the method in field situations. Fluxes were estimated for selected boreholes drilled from the heated tunnel segment in a vertical direction into the surrounding rock. All boreholes showed clearly detectable heat-pipe signatures, as evident from strong temperature gradient changes and extended constant-temperature plateaus. While the measured temperature gradients displayed some data noise, the uncertainty in the flux results caused by this noise was reasonably small, on the order of 25% of the average fluxes. Information on the water saturation in the matrix was developed from boreholes that were equipped with combined temperature and neutron logging devices.

Overall, the magnitude of the heat-driven flux perturbation in the DST was significant, with maximum fluxes as high as 500 mm/yr, which are much larger than the ambient percolation at the site. These results confirm that the decay heat to be emplaced in the geologic repository for nuclear waste at Yucca Mountain will generate significant flux

perturbation in the near-field fractured rock. Strong flux variability was seen between radial boreholes with similar geometry and thermal conditions, but different location along the heated drift segment. This variability is indicative of considerable intermediate-scale heterogeneity in the properties of the fractured porous formation. Regarding further applications, we plan to use the estimated fluxes and their heterogeneity as an additional piece of evidence for calibrating and validating numerical simulation models of the underground heater test at Yucca Mountain.

Acknowledgments

This work was supported by the Director, Office of Civilian Radioactive Waste Management, U.S. Department of Energy, through Memorandum Purchase Order QA-B004220RB3X between Bechtel SAIC Company, LLC and the Ernest Orlando Lawrence Berkeley National Laboratory (Berkeley Lab). The support is provided to Berkeley Lab through the U.S. Department of Energy Contract No. DE-AC03-76SF00098. Review and comments of Christine Doughty, Quanlin Zhou and Dan Hawkes from Berkeley Lab are gratefully appreciated. We also would like to acknowledge the helpful comments of ?? anonymous reviewers.

References

Bechtel SAIC Company, Drift-scale coupled processes (DST and TH Seepage) models, MDL-NBS-HS-000015 REV 01, Bechtel SAIC Company, Las Vegas, Nevada, 2004a.

Bechtel SAIC Company, Thermal testing measurement report, TDR-MGR-HS-000002 REV 00, Bechtel SAIC Company, Las Vegas, Nevada, 2004b.

Birkholzer, J.T. and Y.W. Tsang, Modeling the thermal-hydrologic processes in a large-scale underground heater test in partially saturated fractured tuff, Water Resour. Res., 36(6), 1431-1447, 2000.

Birkholzer, J.T., S. Mukhopadhyay and Y.W. Tsang, Modeling seepage into heated waste emplacement tunnels in unsaturated fractured rock, Vadose Zone J., 3, 819-836, 2004.

Birkholzer, J.T., A temperature-profile method for estimating flow processes in geologic heat pipes, Rep. LBNL-56716 Lawrence Berkeley Natl. Lab., Berkeley, Calif., 2004.

Buscheck, T.A., N.D. Rosenberg, J. Gansemer and Y. Sun, Thermohydrologic behavior at an underground nuclear waste repository, Water Resour. Res., 38(3), 2004.

Bredehoeft, J.D. and I.S. Papadopolous, Rates of vertical groundwater movement estimated from the earth's thermal profile, Water Resour. Res., 1(2), 325-328, 1965.

Constantz, J. and C.L. Thomas, The use of streambed temperature profiles to estimate depth, duration, and rate of percolation beneath arroyos, Water Resour. Res., 32(12), 3597-3602, 1996.

Constantz, J., S.W. Tyler and E. Kwicklis, Temperature-profile methods for estimating percolation rates in arid environments, Vadose Zone J., 2, 12-24, 2003.

Datta, R., D. Barr and W. Boyle, Measuring thermal, hydrological, mechanical, and chemical responses in the Yucca Mountain Drift Scale Test, in: Stephansson, Hudson, Jing, editors, Coupled THMC Processes in Geo-Systems: Fundamentals, Modelling, Experiments & Applications, Elsevier Geo-Engineering Book Series, Oxford, (in press), 155-160, 2004.

Doughty, C. and K. Pruess, A similarity solution for two-phase fluid and heat flow near high-level nuclear waste packages emplaced in porous media, Int. J. Heat Mass Transfer, 33(6), 1205-1222, 1990.

Doughty, C. and K. Pruess, A similarity solution for two-phase water, air, and heat flow near a linear heat source in a porous medium, J. of Geophysical Res., 97(B2), 1821-1838, 1992.

Doughty, C., Investigation of conceptual and numerical approaches for evaluating moisture, gas, chemical, and heat transport in fractured unsaturated rock, J. of Contaminant Hydrology, 38, 69-106, 1999.

Haukwa, C.B., Y.W. Tsang, Y.-S. Wu and G.S. Bodvarsson, Effect of heterogeneity on the potential for liquid seepage into heated emplacement drifts of the potential repository, J. of Contaminant Hydrology, 62-63, 509-527, 2003.

Mukhopadhyay, S. and Y.W. Tsang, Uncertainties in coupled thermal-hydrological processes associated with the Drift Scale Test at Yucca Mountain, J. of Contaminant Hydrology, 62-63, 595-612, 2003.

Pruess, K., J.S.Y. Wang and Y.W. Tsang, On thermohydrologic conditions near high-level nuclear wastes emplaced in partially saturated fractured tuff, 1, Simulation studies with explicit consideration of fracture effects, Water Resour. Res., 26, 1235-1248, 1990a.

Pruess, K., J.S.Y. Wang and Y.W. Tsang, On thermohydrologic conditions near high-level nuclear wastes emplaced in partially saturated fractured tuff, 1, Effective continuum approximations, Water Resour. Res., 26, 1249-1261, 1990b.

Pruess, K., Oldenburg, K. and G. Moridis, TOUGH2 user's guide, Version 2.0, Rep. LBL-43134 Lawrence Berkeley Natl. Lab., Berkeley, Calif., 1999.

Rutqvist, J., C.-F. Tsang and Y.W. Tsang, Analysis of stress- and moisture-induced changes in fractured rock permeability at the Yucca Mountain Drift Scale Test, in: Stephansson, Hudson, Jing, editors, Coupled THMC Processes in Geo-Systems: Fundamentals, Modelling, Experiments & Applications, Elsevier Geo-Engineering Book Series, Oxford, (in press), 161-166, 2004.

Silliman, S.E., J. Ramirez and R.L. McCabe, Quantifying downflow through creek sediments using temperature time series: One-dimensional solution incorporating measured surface temperature, J. of Hydrology, 148(1-4), 99-119, 1995.

Sonnenthal, E.L. and N.F. Spycher, A conceptual and numerical model for thermal-hydrological-chemical processes in the Yucca Mountain Drift Scale Test, in: Stephansson, Hudson, Jing, editors, Coupled THMC Processes in Geo-Systems: Fundamentals, Modelling, Experiments & Applications, Elsevier Geo-Engineering Book Series, Oxford, (in press), 347-352, 2004.

Su, G.W., J. Jasperse, D. Seymour and J. Constantz, Estimation of hydraulic conductivity in an alluvial system using temperatures, Ground Water, 42(6), 890-901, 2004.

Udell, K.S., Heat transfer in porous media considering phase change and capillarity—the heat pipe effect, Int. J. Heat Mass Transfer, 28(2), 485-495, 1985.

van Genuchten, M.T., A closed-form equation for predicting the hydraulic conductivity of unsaturated soils, Soil Science Society of America Journal, 44, (5), 892-898, 1980.

Figures and Tables

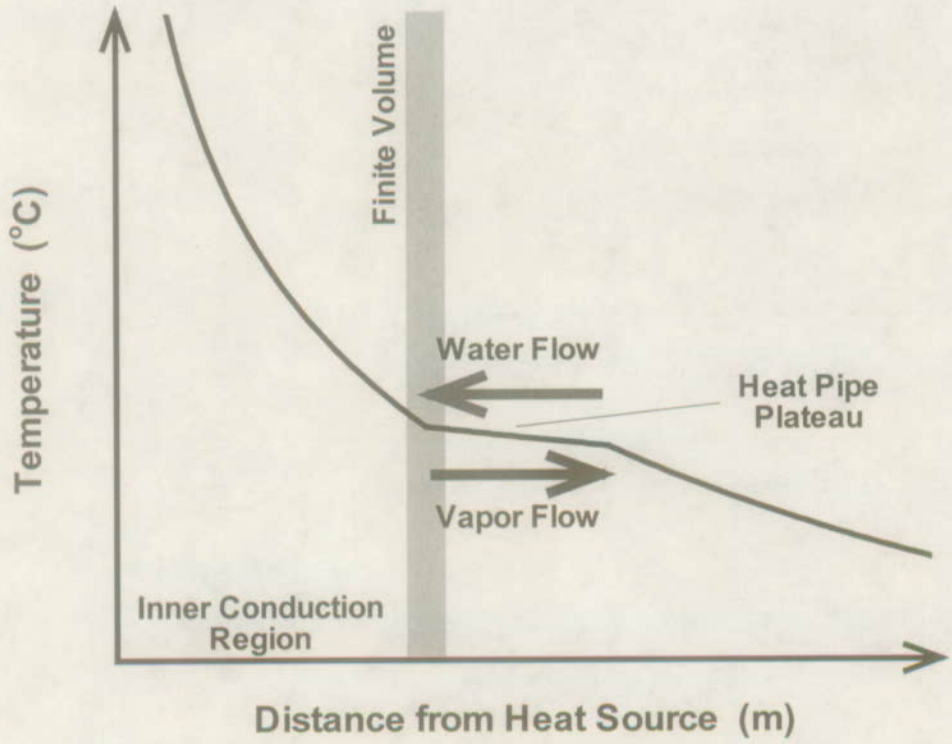

Figure 1: Schematic showing temperature profile with heat pipe signature and definition of finite volume for temperature-profile method

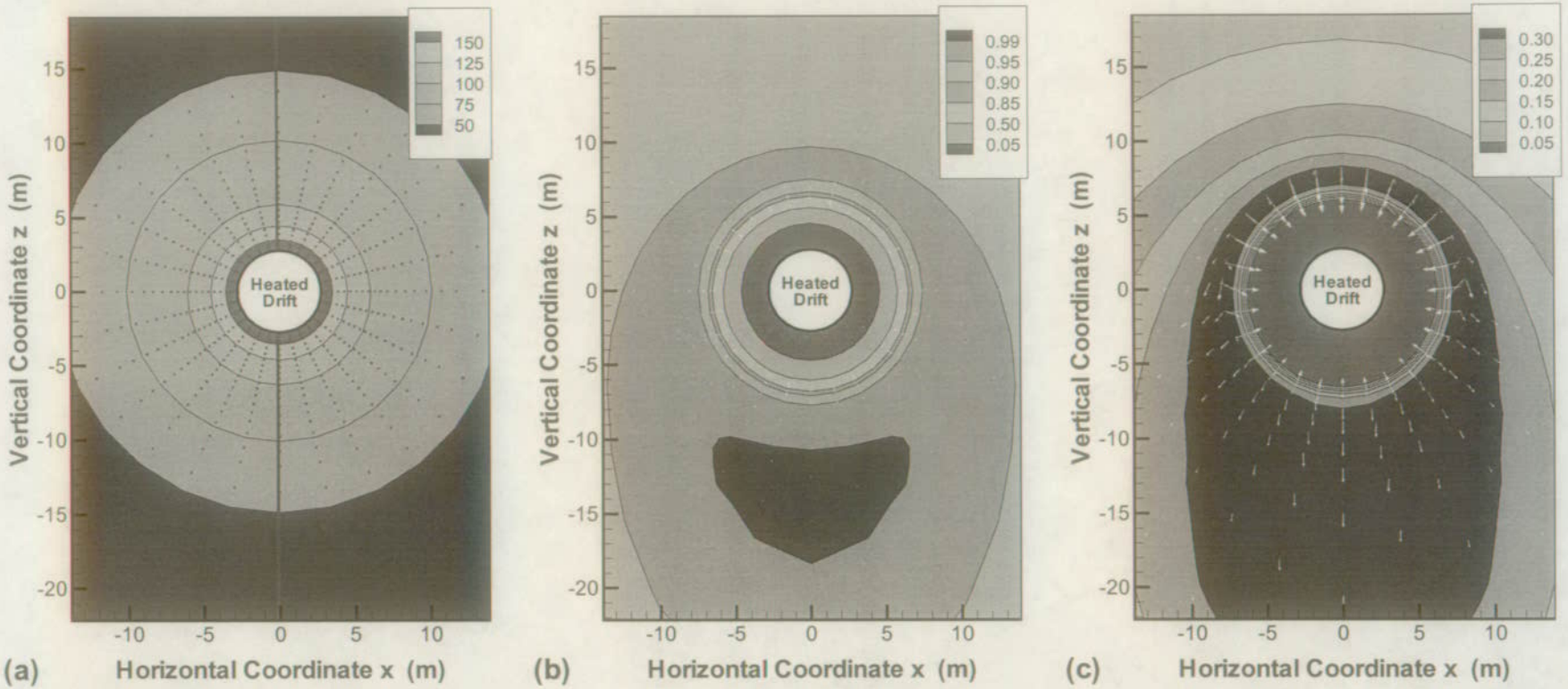

Figure 2. Simulation results for two-dimensional example case at 4 years showing (a) temperature contours in the porous matrix (in °C) and nodal center points of finite volume discretization, (b) liquid saturation contours plus liquid flux vectors in the porous matrix, and (c) liquid saturation and liquid flux vectors in the fracture continuum. The temperature contours in the fracture continuum are virtually identical to those in the matrix. Vector length is proportional to flux, with the same proportionality factor for matrix and fracture fluxes. Red lines in temperature plot indicate profiles chosen for temperature-profile analysis (vertical up and vertical down).

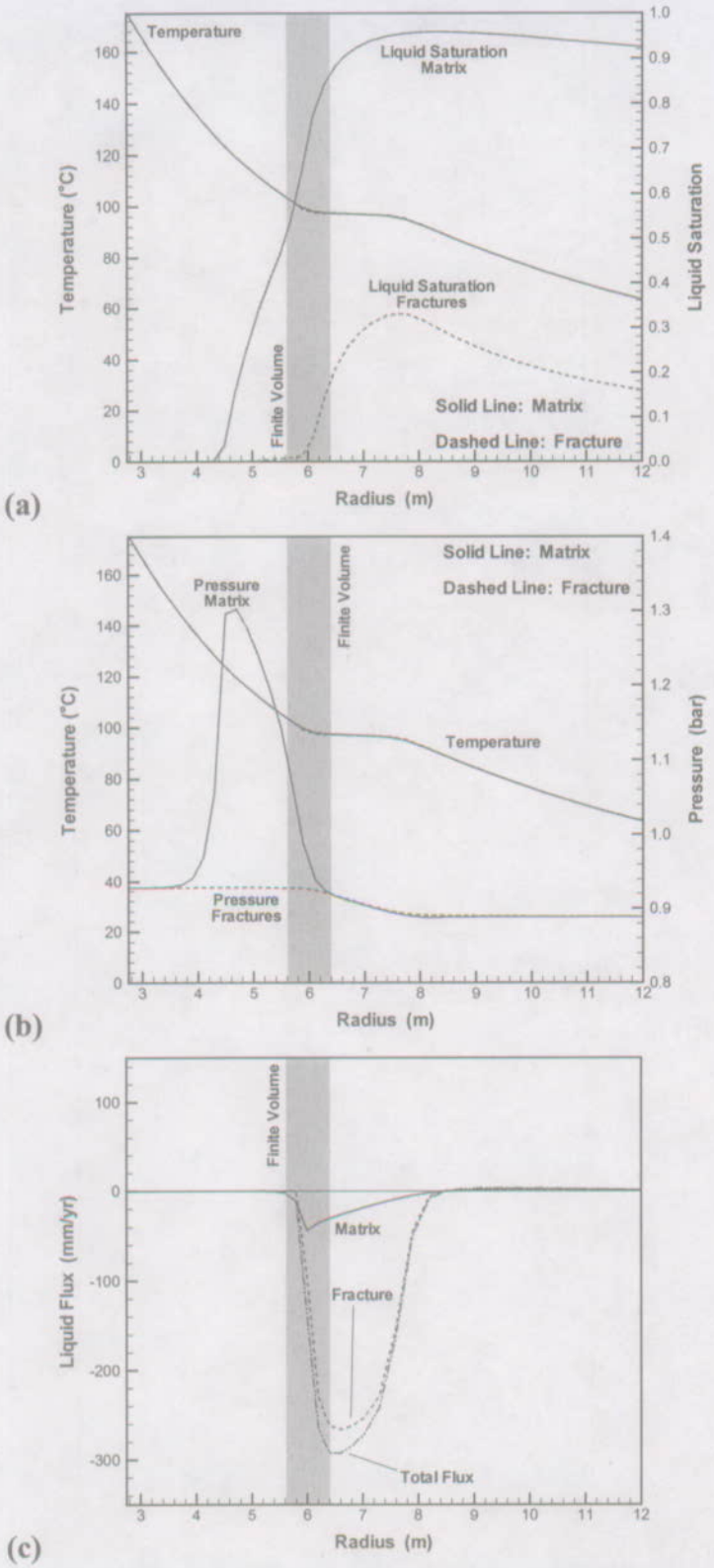

Figure 3. Simulation results for two-dimensional example case, showing profiles at 4 years for the vertical borehole above the heater. Plots show (a) temperature and liquid saturation, (b) temperature and gas pressure, and (c) liquid fluxes. The tunnel wall is at radius r = 2.75 m.

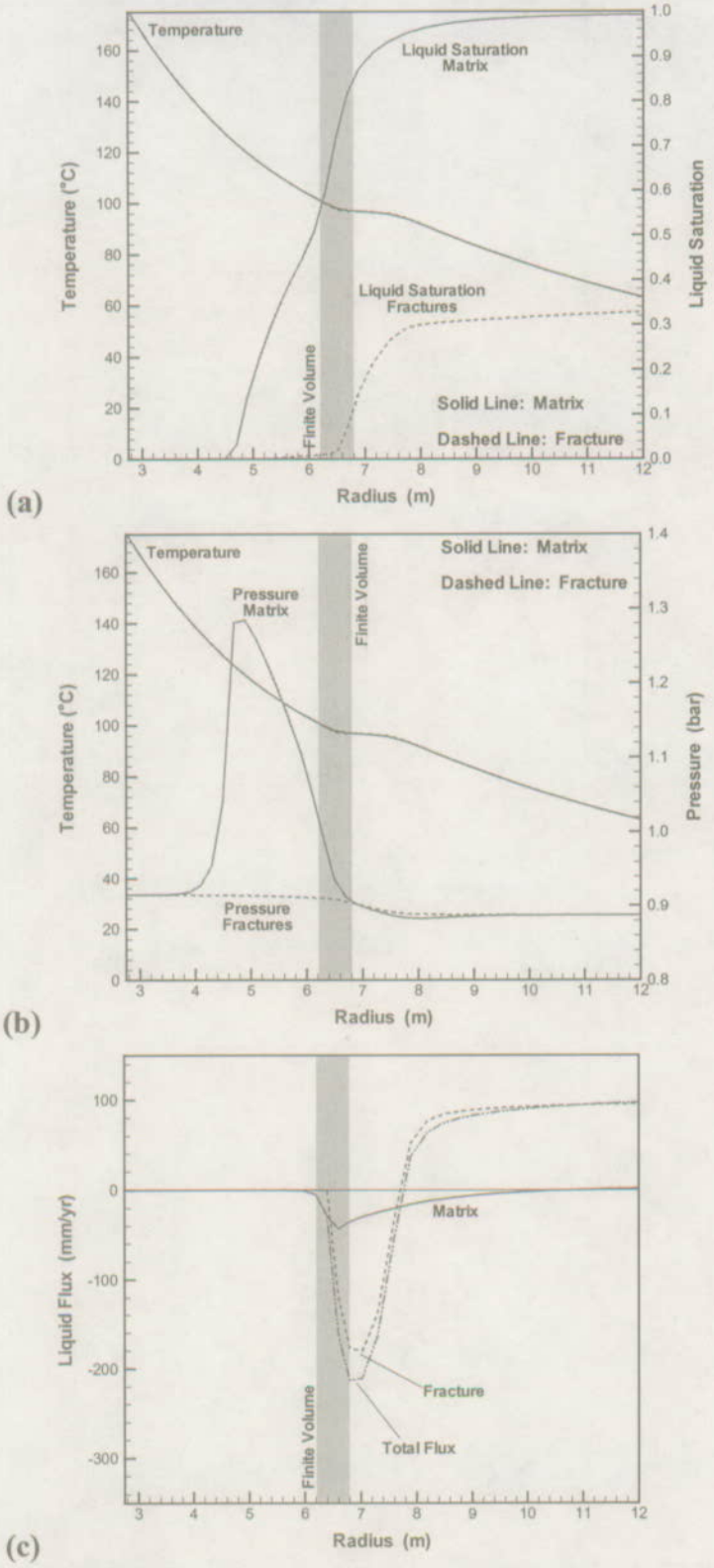

Figure 4. Simulation results for two-dimensional example case, showing profiles at 4 years for the vertical borehole below the heater. Plots show (a) temperature and liquid saturation, (b) temperature and gas pressure, and (c) liquid fluxes. The tunnel wall is at radius r = 2.75 m.

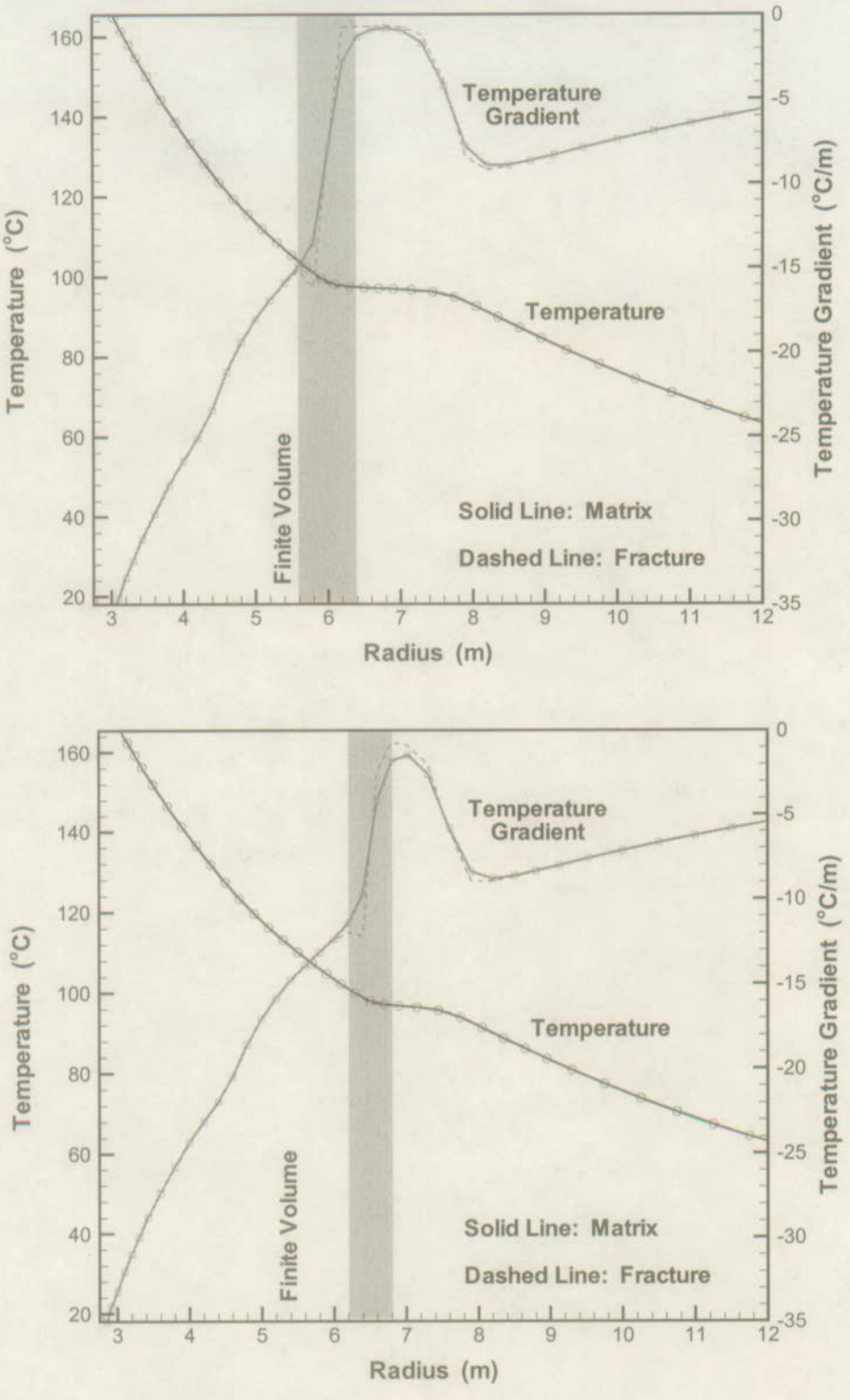

Figure 5. Temperature-profile method for two-dimensional example case, showing profiles at 4 years for (a) the vertical borehole above and (b) the vertical borehole below the heater. Plot shows simulated temperature at nodal points, average gradient between two adjacent nodal points, and choice of finite volume. The tunnel wall is at radius r = 2.75 m.

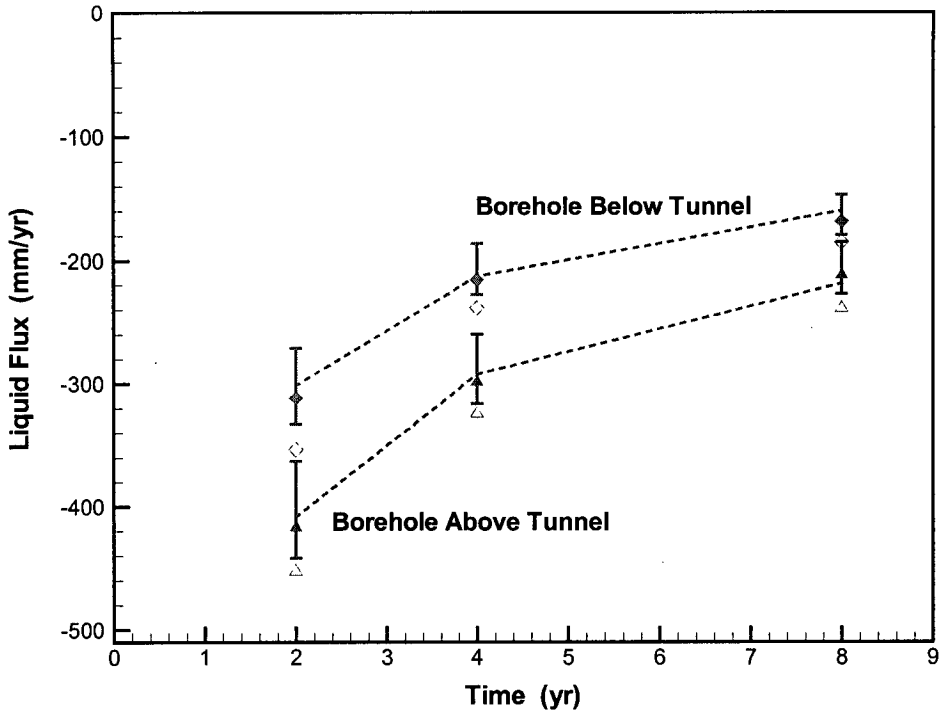

Figure 6. Flux estimates from temperature-profile method for two-dimensional example case in comparison with simulated fluxes. Hollow symbols give estimated fluxes using the quasi-steady heat pipe solution. Solid symbols give estimated fluxes using the transient heat pipe solution. Error bars give range of transient flux results calculated using the dry thermal conductivity and the wet thermal conductivity. Dashed lines connect simulated flux values.

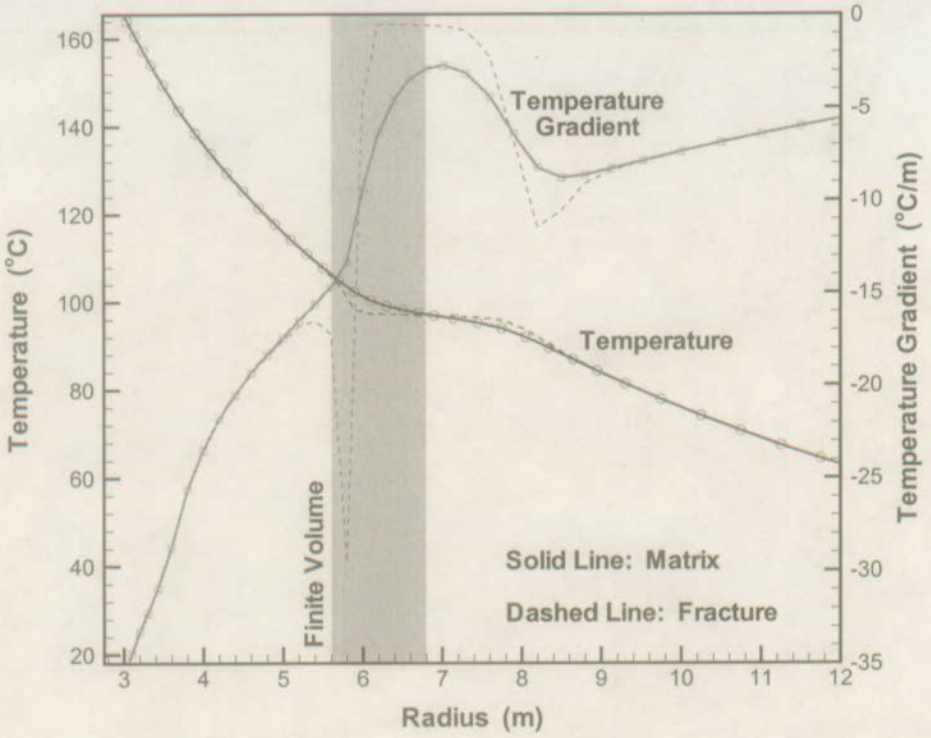

(a)

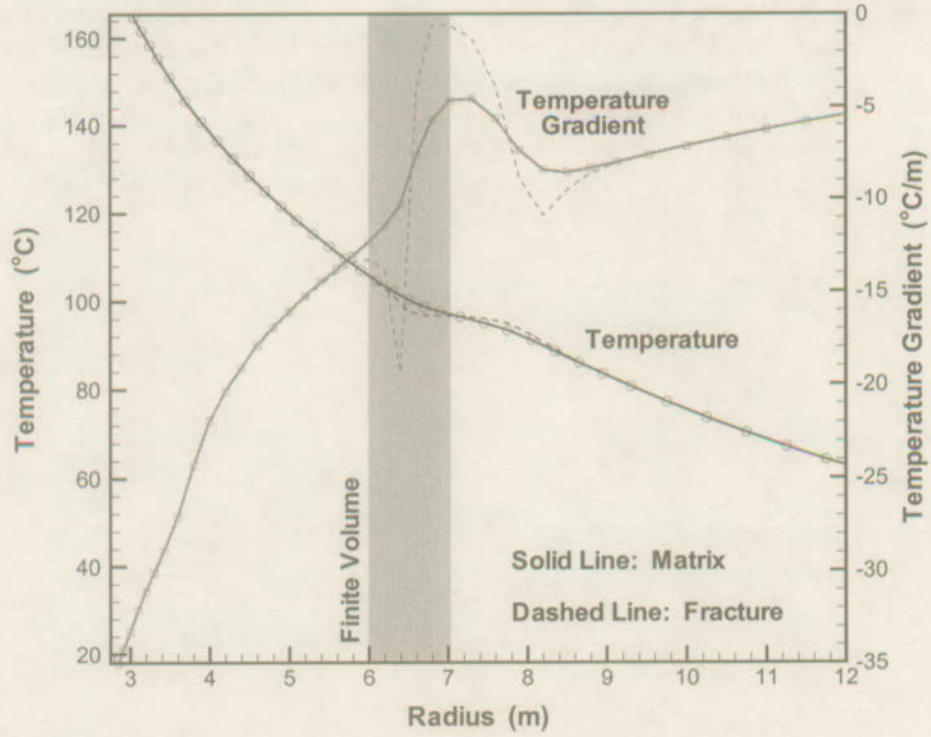

(b)

Figure 7. Temperature-profile method for two-dimensional example case with reduced interfacial area, showing profiles at 4 years for (a) the vertical borehole above and (b) the vertical borehole below the heater. Plot shows simulated temperature at nodal points, average gradient between two adjacent nodal points, and choice of finite volume. The tunnel wall is at radius r = 2.75 m.

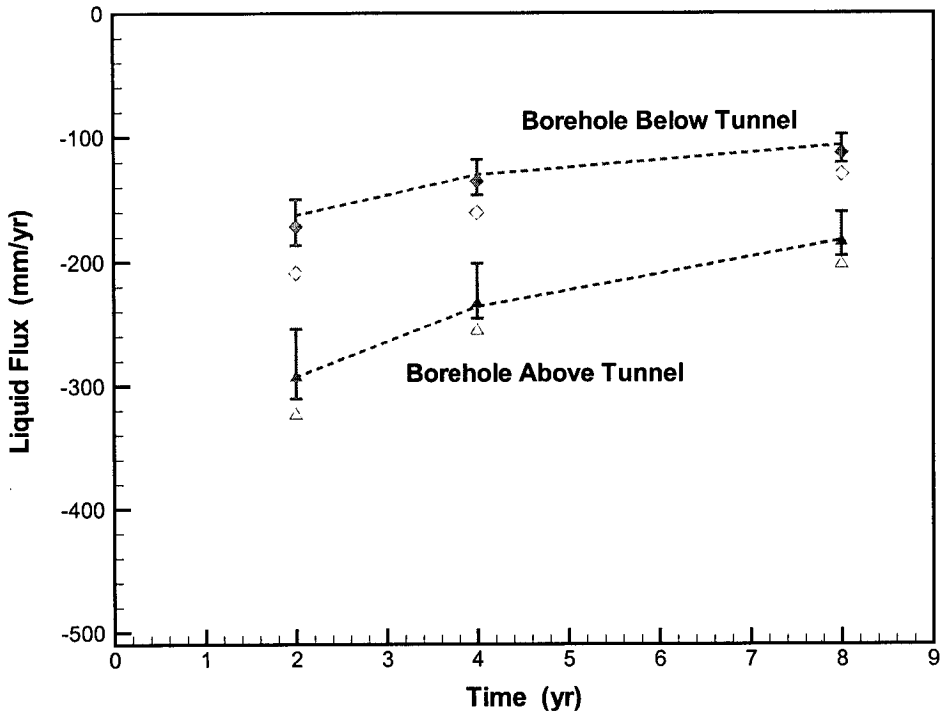

Figure 8. Flux estimates from temperature-profile method for two-dimensional example case with reduced interfacial area in comparison with simulated fluxes. Hollow symbols give estimated fluxes using the quasi-steady heat pipe solution. Solid symbols give estimated fluxes using the transient heat pipe solution. Error bars give range of transient flux results calculated using the dry thermal conductivity and the wet thermal conductivity. Dashed lines connect simulated flux values.

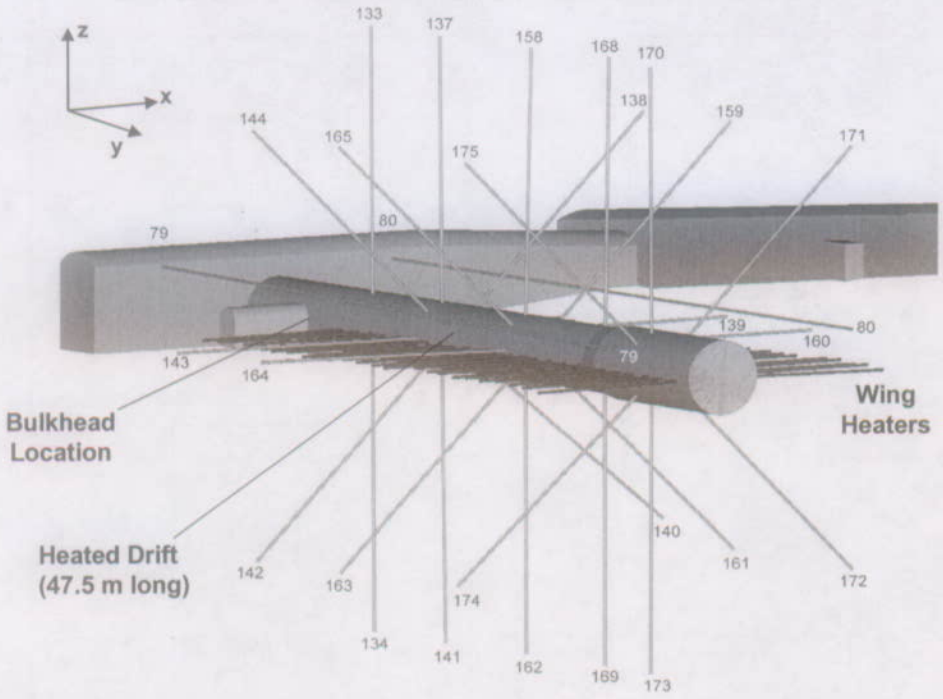

(a)

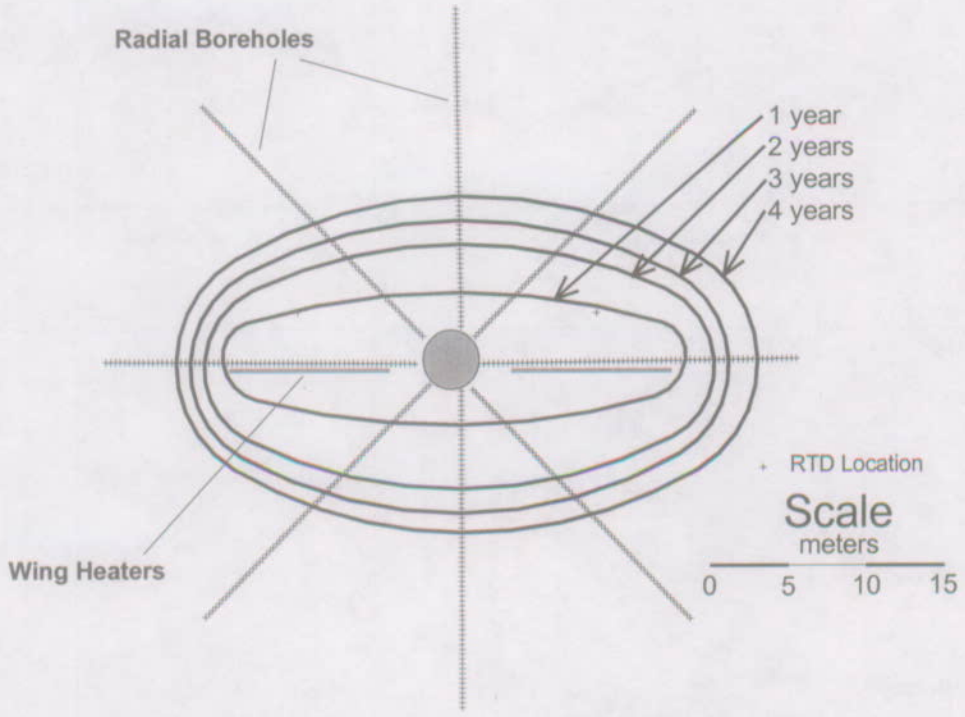

(b)

Figure 9: (a) Three-dimensional perspective of heated drift section (round tunnel) of the DST connected with access tunnels. The length of the heated drift is 47.5 m from the bulkhead to the end. (b) Sample array of boreholes in radial cluster orthogonal to heated drift. Boreholes oriented vertically up and down are chosen for temperature-profile method. Contours show 95°C isotherm at 1, 2, 3, and 4 years of heating, interpolated from measured borehole data (from BSC 2004).

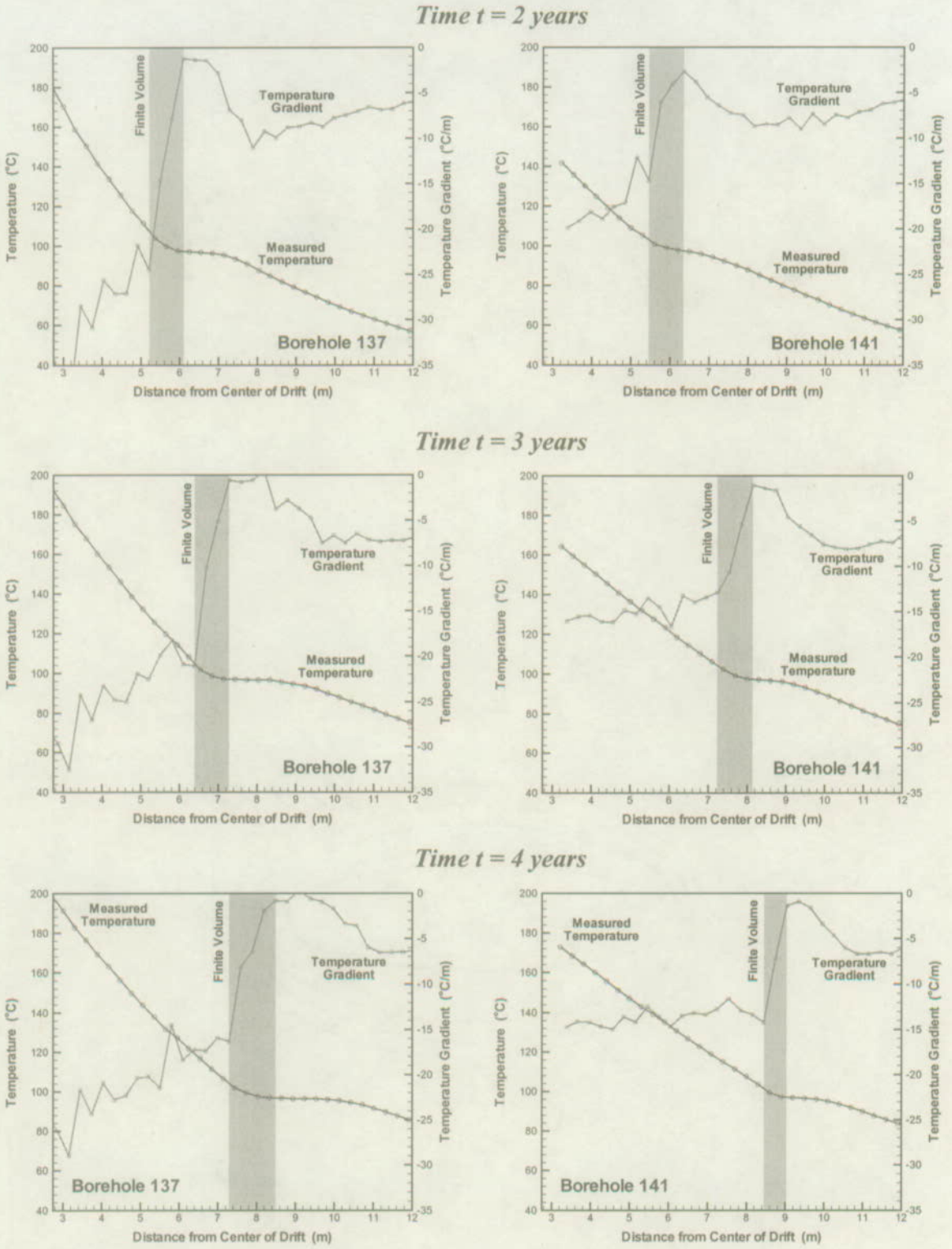

Figure 10: DST temperatures measured at 2, 3, and 4 years of heating in Borehole 137 (vertically up) and Borehole 141 (vertically down). Plot shows measured temperature at sensor location (given in radial distance from drift center), average gradient between two adjacent sensors, and choice of finite volume for temperature-profile method.

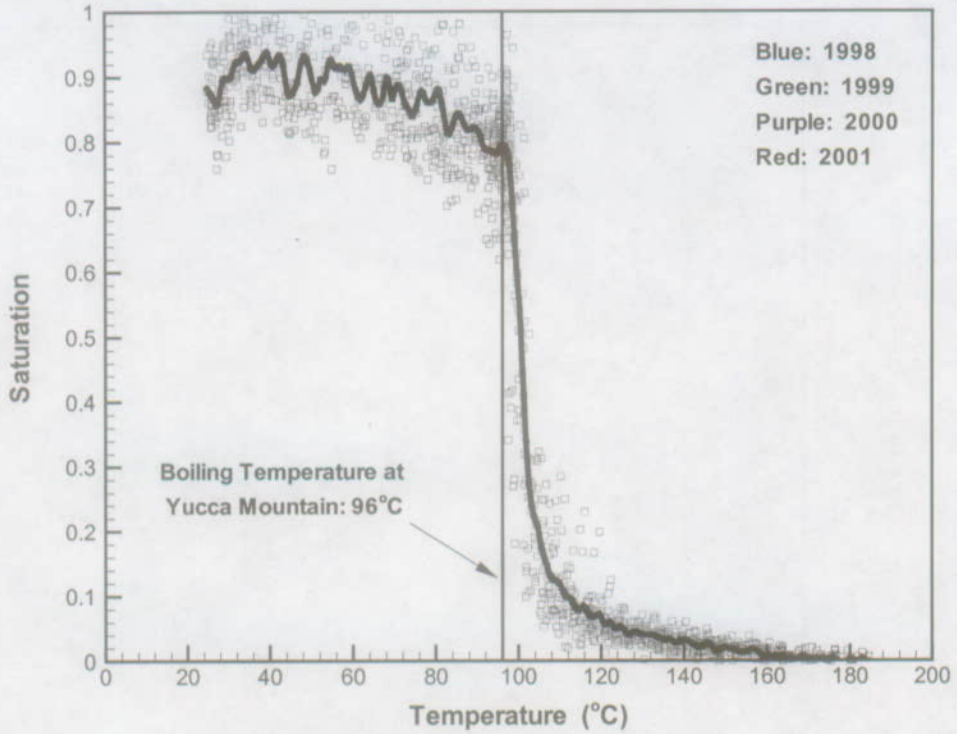

Figure 11: Saturation versus temperature measured from Borehole 79 (horizontal along heated drift). Borehole is equipped with a combined RTD and neutron logging device. The moisture content estimated from the neutron logging analysis is converted into water saturation using the porosity of the tuff matrix. The color coding indicates the year in which measurement was conducted. The heavy black line is produced by a smoothing algorithm using a smoothing interval of 2°C.

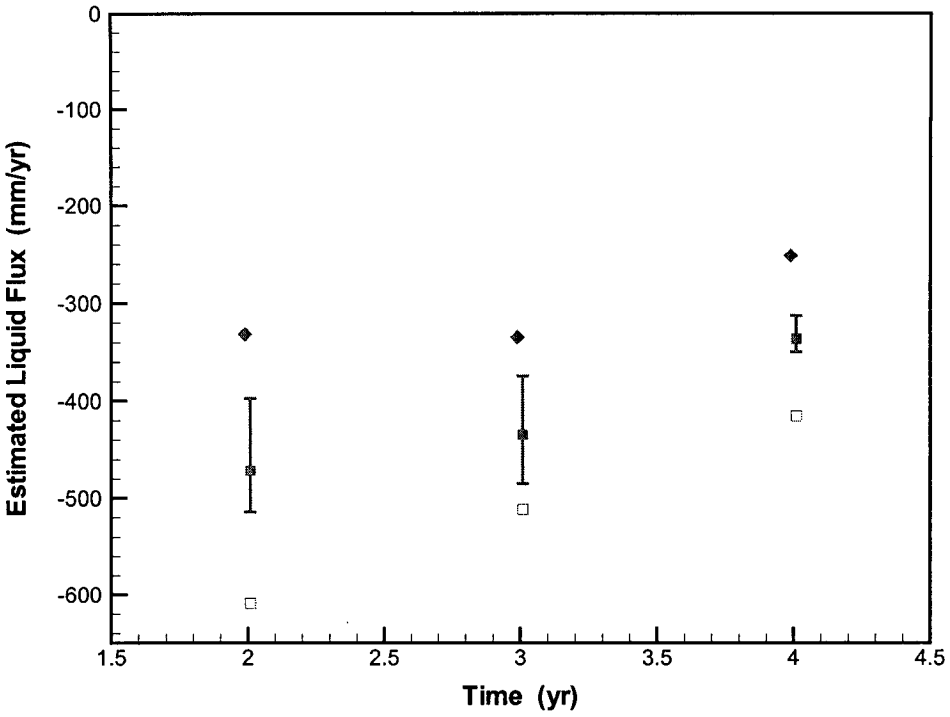

(a)

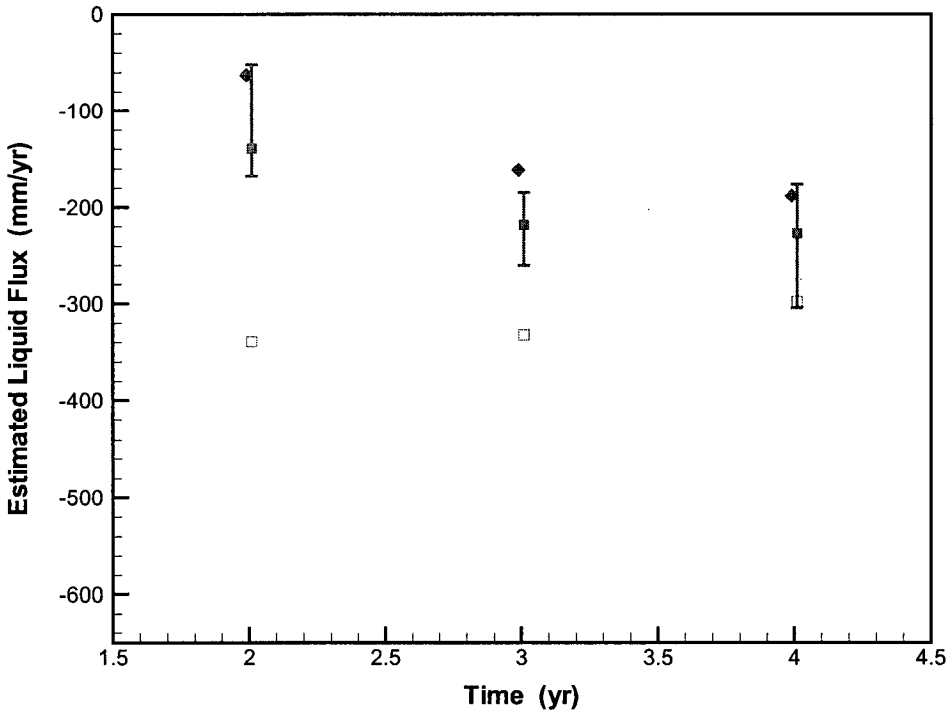

(b)

Figure 12: Flux estimates from temperature-profile method for DST temperatures measured in (a) Borehole 137 (vertically up) and (b) Borehole 141 (vertically down). Results in blue are for linear heat pipe solution; results in red are for radial heat pipe solution. Solid symbols give average transient fluxes over five upstream locations. Error bars indicate range of five individual transient flux estimates. Hollow symbols show average steady-state fluxes.

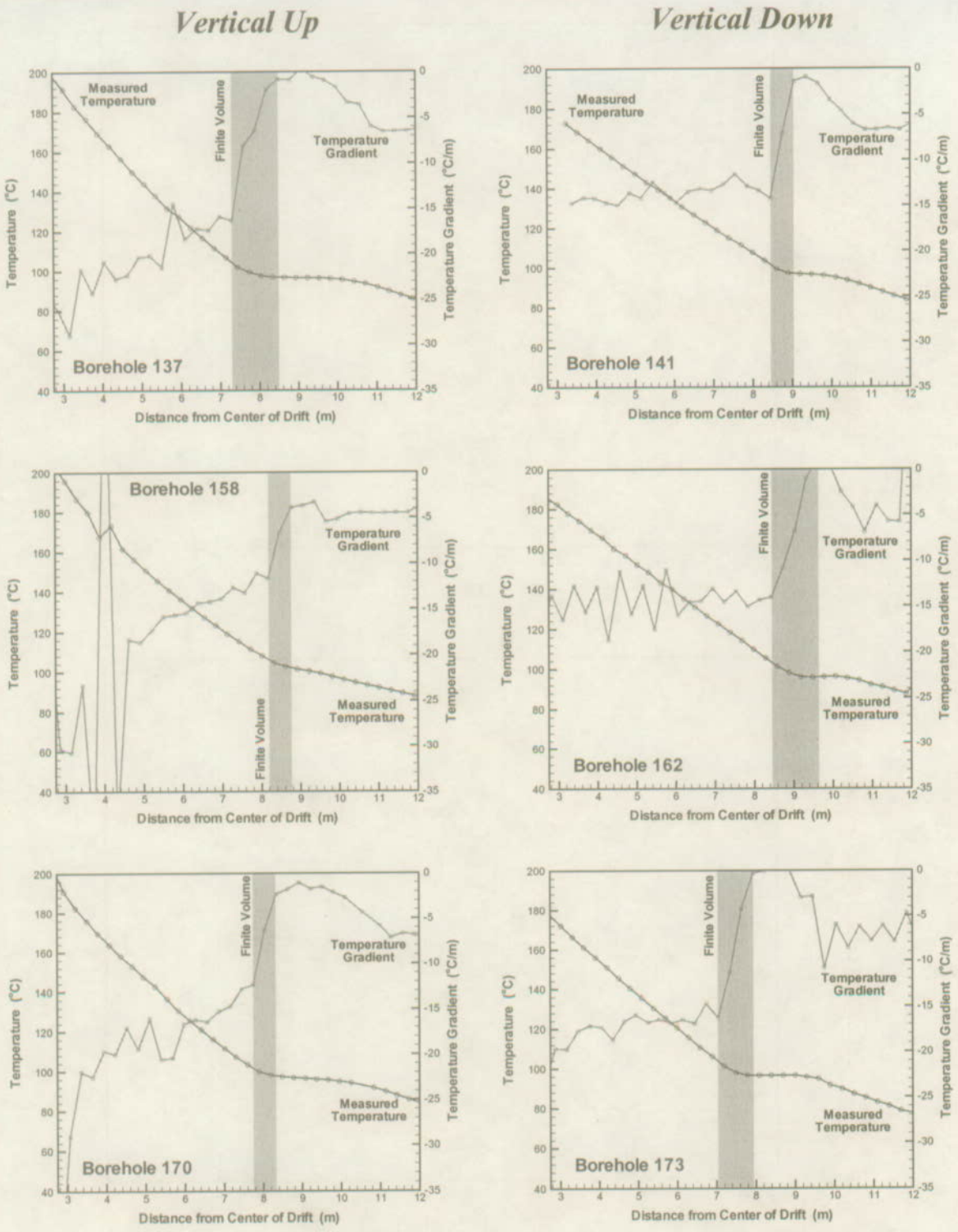

Figure 13: DST temperatures measured at 4 years of heating in Boreholes 137, 158, and 170 (vertically up) and Boreholes 141, 162, and 173 (vertically down). Plot shows measured temperature at sensor location (given in radial distance from drift center), average gradient between two adjacent sensors, and choice of finite volume for temperature-profile method.

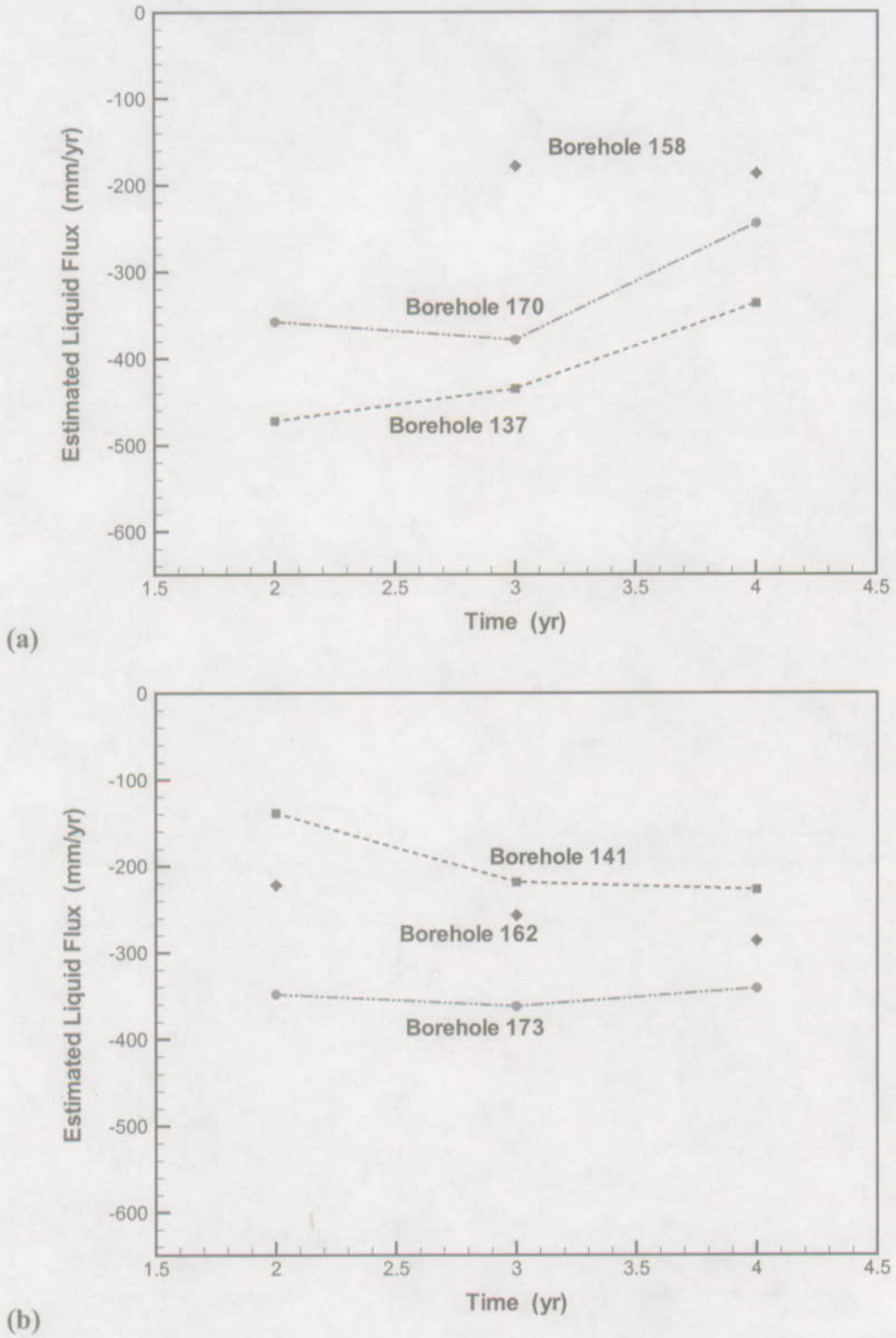

Figure 14: Comparison of flux estimates from temperature-profile method for DST temperatures measured in (a) all boreholes oriented vertically up and (b) all boreholes oriented vertically down. Plot shows results from transient heat pipe solution for linear geometry. There are no flux results for Borehole 158 at 2 years, since no clear heat pipe signature was detectable.

Table 1: Hydrogeological and Thermal Input Values

Parameter	Value
Material Properties	
Matrix Permeability	1.24×10^{-16} m^2
Matrix Porosity	0.11
Matrix Grain Density	2530 kg/m^3
Matrix Grain Heat Capacity	952.9 J/kg/K
Matrix Dry Thermal Conductivity	1.67 W/m/K
Matrix Wet Thermal Conductivity	2.0 W/m/K
Fracture Permeability	1.0×10^{-13} m^2
Volume Fraction of Fractures	0.000263
Binary diffusion coefficient	2.14×10^{-5} m^2/s (at standard conditions)
Tortuosity	0.2
Temperature Exponent	2.334
Fracture Geometry Assumed for Dual-Continuum Formulation	
Fracture-Matrix Interface Area	3.76 m^2 per unit volume of rock
Average Distance from Fracture to Matrix Block Center	0.089 m
Characteristic Curves	
Matrix Residual Liquid Saturation	0.18
Matrix Van Genuchten Parameter, 1/α	4.444 bar
Matrix Van Genuchten Parameter, m	0.247
Fracture Residual Liquid Saturation	0.01
Fracture Van Genuchten Parameter, 1/α	0.103 bar
Fracture Van Genuchten Parameter, m	0.492
Maximum Capillary Pressure P_{max}	1000 bar

Note: The above list is based primarily on the property set developed for the Topopah Spring Middle Nonlithophysal Unit close to the location of the drift scale test at Yucca Mountain (from Birkholzer and Tsang, 2000). Binary diffusion is calculated in dependence of pressure and temperature according to Pruess et al. (1999), using the binary diffusion coefficient at standard conditions, the tortuosity factor , and the temperature exponent as inputs. The characteristic curves utilize the functional forms introduced by van Genuchten (1980), with a slight modification regarding the maximum possible capillary pressure. The saturation-dependent thermal conductivity in the matrix is calculated from: $\lambda(S_L) = \lambda_{dry} + (\lambda_{wet} - \lambda_{dry}) S_L^{0.5}$, where S_L is liquid saturation, λ_{dry} is the thermal conductivity of oven-dried samples, and λ_{wet} is the thermal conductivity of water-saturated samples.

Appendix A: Details on the Flux Calculations with the Temperature-Profile Method

Table A1: Application of temperature-profile method to two-dimensional example (base case)

Bore-hole	Time	Finite Volume Radii		Matrix Temperature		Matrix Temperature Gradient		Matrix Saturation		Matrix Thermal Conductivity		Boiling Front Velocity	Quasi-steady Liquid Flux	Transient Liquid Flux	Simul. Transient Liquid Flux (F + M)
	t	r_1	r_2	T_2	T_2	∇T_2	∇T_2	$S_{L,1}$	$S_{L,2}$	λ_1	λ_2	$\dot{v}$	q_L^S	q_L^T	$q_L^T(sim)$
	yr	m		°C		°C/m		–		W/(m-K)		m/yr	mm/yr	mm/yr	mm/yr
Vertical Up	2	4.0	4.8	106.0	97.3	-21.7	-1.7	0.50	0.87	1.90	1.98	0.79	-453	-417	-409
Vertical Up	4	5.6	6.4	103.9	97.4	-14.9	-1.3	0.50	0.86	1.90	1.98	0.60	-325	-298	-293
Vertical Up	8	7.6	8.8	105.3	97.3	-11.0	-0.8	0.43	0.86	1.89	1.98	0.53	-239	-212	-219
Vertical Down	2	4.2	5.0	105.4	96.9	-18.1	-3.1	0.49	0.87	1.90	1.98	0.91	-354	-312	-301
Vertical Down	4	6.2	6.8	101.1	97.0	-11.5	-1.9	0.55	0.85	1.92	1.97	0.66	-238	-216	-213
Vertical Down	8	8.5	9.5	102.0	96.9	-8.6	-1.0	0.49	0.83	1.90	1.97	0.41	-185	-169	-160

Note: Table values have been rounded, while more digits have been used for calculations. This may cause minor inconsistencies between input and output values. Boiling front velocities were calculated using additional temperature profiles at 3 months prior to and after the target time.

Table A2: Application of temperature-profile method to two-dimensional example with reduced fracture-matrix interface area

Bore-hole	Time	Finite Volume Radii		Matrix Temperature		Matrix Temperature Gradient		Matrix Saturation		Matrix Thermal Conductivity		Boiling Front Velocity	Quasi-steady Liquid Flux	Transient Liquid Flux	Simul. Transient Liquid Flux (F + M)
	t	r_1	r_2	T_2	T_2	∇T_2	∇T_2	$S_{L,1}$	$S_{L,2}$	λ_1	λ_2	$\dot{v}$	q_L^S	q_L^T	$q_L^T(sim)$
	yr	m		°C		°C/m		–		W/(m-K)		m/yr	mm/yr	mm/yr	mm/yr
Vertical Up	2	4.0	5.0	110.1	97.6	-21.6	-5.6	0.60	0.88	1.93	1.98	0.79	-324	-293	-293
Vertical Up	4	5.6	6.8	106.5	97.3	-14.7	-2.9	0.60	0.88	1.93	1.98	0.61	-256	-234	-236
Vertical Up	8	7.6	8.8	105.3	97.3	-11.0	-0.8	0.43	0.86	1.89	1.98	0.53	-239	-212	-219
Vertical Down	2	4.2	5.2	108.8	96.3	-18.6	-7.3	0.58	0.87	1.92	1.98	0.92	-209	-172	-163
Vertical Down	4	6.0	7.0	105.9	97.0	-12.4	-4.7	0.57	0.86	1.92	1.98	0.66	-161	-136	-130
Vertical Down	8	8.5	10	104.0	96.2	-8.6	-2.6	0.56	0.87	1.92	1.98	0.44	-130	-113	-107

Note: Table values have been rounded, while more digits have been used for calculations. This may cause minor inconsistencies between input and output values. Boiling front velocities were calculated using additional temperature profiles at 3 months prior to and after the target time.